NOAA FISHERIES

Updated model-based abundance estimates of pelagic false killer whales in Hawaiian waters and the broader central Pacific

Janelle J. Gardner, Devin S. Johnson, Amanda L. Bradford, Yvonne M. Barkley, Elizabeth A. Becker, & Erin M. Oleson

NOAA Technical Memorandum TM-PIFSC-189
U.S. Department of Commerce
National Oceanic and Atmospheric Administration
National Marine Fisheries Service
Pacific Islands Fisheries Science Center
August 2026

Updated model-based abundance estimates of pelagic false killer whales in Hawaiian waters and the broader central Pacific

Janelle J. Gardner[1], Devin S. Johnson[1], Amanda L. Bradford[1], Yvonne M. Barkley[2], Elizabeth A. Becker[3], & Erin M. Oleson[1]

[1] Pacific Islands Fisheries Science Center
National Marine Fisheries Service
1845 Wasp Boulevard
Honolulu, HI 96818

[2] Cooperative Institute for Marine and Atmospheric Research
Research Corporation of the University of Hawai‘i
Honolulu, HI 96822

[3] Cascadia Scientific Services, LLC
Olympia, WA 98501

NOAA Technical Memorandum TM-PIFSC-189
August 2026

U.S. Department of Commerce
National Oceanic and Atmospheric Administration
National Marine Fisheries Service
Pacific Islands Fisheries Science Center

Acknowledgements

We gratefully acknowledge the dedicated efforts of the survey coordinators, observers, acousticians, and the officers and crew aboard each of the Pacific Islands Fisheries Science Center (PIFSC) and Southwest Fisheries Science Center (SWFSC) surveys that contributed data to this analysis.

The Hawaiian Islands Cetacean Assessment Survey (HICEAS) 2002 was funded by SWFSC, and HICEAS 2010 was funded by SWFSC and PIFSC, with additional contributions by the Pacific Islands Regional Office and the NOAA Fisheries National Take Reduction Program. HICEAS 2017 was conducted as part of the Pacific Marine Assessment Program for Protected Species (PacMAPPS), a collaborative effort between NOAA Fisheries, the U.S. Navy, and the Bureau of Ocean Energy Management (BOEM) to collect data necessary to produce updated abundance estimates for cetaceans in Hawaiian waters. BOEM funding was provided via Interagency Agreement (IAA) M17PG00024 and M17PG00025, and Navy funding via IAAs with Chief of Naval Operations N45 (NEC-16-011-01BP) and Pacific Fleet Environmental Readiness Division (NMFS-PIC-07-006). Additional contributions were provided by the NMFS Office of Science and Technology, the National Take Reduction Program, and the National Seabird Program. HICEAS 2023 was executed with funding from PIFSC and PacMAPPS partner BOEM (BOEM Agreement Number NSL PC-23-02a; NOAA Agreement Number NMFS-PIC-23-003).

Survey effort within the Papahānaumokuākea Marine National Monument was conducted under research permits PMNM-2010-53, PMNM-2017-17, and PMNM-2023-01. False killer whales were approached and sampled during HICEAS efforts under NMFS MMPA-ESA take permits 774-1437 (in 2002) and 14097 (in 2010) issued to SWFSC and 20311 (in 2017) and 25754 (in 2023) issued to PIFSC.

Annette Henry was the survey coordinator for HICEAS 2002 and 2010. HICEAS 2017 and 2023 were coordinated by Kym Yano, with assistance from Annette Henry. We are indebted to the contributions of Karin Forney in developing and executing the approaches for false killer whale data collection, abundance estimation, and density surface modeling reflected in this effort. This work was made possible by funding from the NOAA Fisheries National Protected Species Toolbox Initiative and the National Take Reduction Program. This report was greatly improved from technical reviews by Phil Bouchet, Milani Chaloupka, Jason Roberts, and the Pacific Scientific Review Group.

Mention throughout this document to trade names or commercial companies is for identification purposes only and does not imply endorsement by the National Marine Fisheries Service, NOAA.

Edited by Revere Wood.

Data and Code Availability Statement

Data and code are available in an online repository and associated vignette.

Recommended citation

Gardner, J., Johnson, D., Bradford, A., Barkley, Y., Becker, E., and Oleson, E. (2026). Updated model-based abundance estimates of pelagic false killer whales in Hawaiian waters and the broader central Pacific. (Technical Memorandum Series, TM-PIFSC-189). Pacific Islands Fisheries Science Center.

Copies of this report are available from

Pacific Islands Fisheries Science Center
National Marine Fisheries Service
National Oceanic and Atmospheric Administration
1845 Wasp Boulevard, Building #176
Honolulu, Hawai‘i 96818

Or online at

https://repository.library.noaa.gov/

Table of Contents

List of Tables

List of Figures

Executive Summary

False killer whales (*Pseudorca crassidens*) are broadly distributed in pelagic waters of the central Pacific, where they depredate and are vulnerable to bycatch in commercial longline fisheries. To support the assessment and management of the Hawai‘i pelagic false killer whale population, we estimated the abundance of the pelagic false killer whales in Hawaiian waters and the broader central Pacific using spatially-explicit habitat-based density modeling.

We used encounter data from 40 ship-board line-transect surveys conducted by the Southwest Fisheries Science Center and Pacific Islands Fisheries Science Center in the central and eastern Pacific during 1986–2023, resulting in 135 false killer whale sightings used to derive detectability parameters. Our density surface model was fit to a subset of these data; specifically, 44 sightings from 14,399 10-km survey segments over 20 line-transect surveys in the central Pacific during 1997–2023. The most supported models for encounter rate and group size included a tensor product smooth of latitude and sea surface temperature for encounter rate and sea surface height and mixed layer depth for group size. This model output was used to predict abundance estimates for pelagic false killer whales from 2020–2024 in three regions: the full central Pacific study area, the Hawai‘i pelagic false killer whale assessment area, and the U.S. Exclusive Economic Zone around the Hawaiian Islands (Hawaiian EEZ). The average estimated abundance from 2020–2024 is 33,216 pelagic false killer whales (95% confidence interval (CI): [9,917–82,950]) in the broader central Pacific, 4,526 (95% CI: [1,547–10,444]) in the assessment area, and 1,745 (95% CI: [526–4,334]) in the Hawaiian EEZ.

The modeling framework we used is an update from previous efforts to estimate pelagic false killer whale abundance in these regions, incorporating recent technical and statistical advances. Methodological improvements include refined oceanographic products for modeling, enhanced spatially-explicit propagation of uncertainty in detection and encounter rate parameters, posterior bootstrapping to incorporate group size uncertainty, weighted likelihood proration of population identity, and clamping to address extrapolation effects. The updated workflow is presented as a unified framework with modernized code in a public repository for increased accessibility, transparency, and reproducibility in support of management activities involving Hawai‘i pelagic false killer whales.

Introduction

False killer whales (*Pseudorca crassidens*) are large toothed whales that inhabit sub-tropical and tropical oceanic domains worldwide and are considered rare throughout their range (Zaeschmar & Baird, 2026). Three distinct and overlapping populations of false killer whales are found within the waters of the U.S. Exclusive Economic Zone (EEZ) around the Hawaiian Islands (Hawaiian EEZ): two insular populations, one around the main Hawaiian Islands (MHI) and the other around the Northwestern Hawaiian Islands (NWHI), and a wide-ranging Hawai‘i pelagic population (e.g., Baird et al., 2008; Baird et al., 2010; Baird et al., 2012; Baird et al., 2013; Bradford et al., 2015). Despite their overlapping ranges, numerous studies have differentiated these populations using photo-identification, genetic sampling, and satellite tagging (e.g., Baird et al., 2008; Baird et al., 2010; Baird et al., 2013; Martien et al., 2014; Oleson et al., 2010; Oleson et al. 2023).

The Hawai‘i pelagic false killer whale population extends beyond the Hawaiian EEZ and experiences a greater degree of overlap with commercial longline fisheries associated with both U.S. and foreign fleets (Ahrens et al., 2025; Oleson et al., 2023). This population is known to depredate bait and catch in the Hawai‘i pelagic longline fisheries (Bayless et al., 2017; Fader et al., 2021; Forney et al., 2011). The resulting bycatch of Hawai‘i pelagic false killer whales has long exceeded allowable levels (first noted in Carretta et al., 2009), leading to the formation of a Take Reduction Team in 2010 and Take Reduction Plan in 2012[1] to reduce serious injury and mortality of false killer whales from fishing operations, in accordance with the Marine Mammal Protection Act.

Prior to 2023, the Hawai‘i pelagic false killer whale population was assessed and managed within the Hawaiian EEZ, where survey effort is concentrated. However, following updated NOAA Fisheries guidelines for assessing marine mammal stocks (NMFS, 2023), an assessment area beyond the EEZ was developed to better represent the geographic range of Hawai‘i pelagic false killer whales and allow for a more comprehensive evaluation of fishery impacts on this population (Oleson et al., 2023). The Hawai‘i pelagic false killer whale assessment area is defined as a minimum convex polygon of a 35 km buffer around all genetic, telemetry, sighting, and bycatch location data known or assumed to be of Hawai‘i pelagic false killer whales (Figure 1). Assessing the distribution and abundance of Hawai‘i pelagic false killer whales in this area is necessary for ongoing efforts to measure and mitigate impacts from fisheries interactions.

[1] 77 Federal Register 71260 (29 November 2012)

Abundance estimation for Hawai‘i pelagic false killer whales has included design- and model-based approaches using encounters from multiple ship-based line-transect surveys (Bradford et al., 2020). The majority of these data come from surveys conducted by the Pacific Islands Fisheries Science Center (PIFSC) in and adjacent to the Hawaiian EEZ (e.g., the Hawaiian Islands Cetacean Assessment Survey, or HICEAS; Yano et al. 2025), as well as surveys conducted by the Southwest Fisheries Science Center (SWFSC) in the Hawaiian EEZ and broader central Pacific (e.g., Hamilton et al., 2009). When a properly randomized survey design is implemented, design-based estimates from these line-transect surveys are theoretically unbiased (Thomas et al., 2007). However, this approach only estimates an average density for a study area or survey stratum, which is limiting for management scenarios that require spatially-explicit estimates at finer scales. Additionally, for Hawai‘i pelagic false killer whales in the Hawaiian EEZ, design-based estimates were found to be highly variable due to random variation in encounter rate and shifts in distribution within and around the EEZ (Bradford et al., 2020).

Model-based frameworks, alternatively, can link animal observations to habitat characteristics to predict densities on a finer spatial scale, while relaxing some of the requirements of survey design (Hedley & Buckland, 2004; Miller et al., 2013). Subsequently, these density-habitat relationships may be used to predict beyond the temporal and spatial bounds of sampling (e.g., Becker et al., 2014; Mannocci et al., 2015; Bouchet et al., 2019). As Hawai‘i pelagic false killer whales range beyond the Hawaiian EEZ, where PIFSC survey effort has focused, a model-based approach allows estimation of their density and abundance in the population’s full assessment area (as presented in Oleson et al., 2023).

Bradford et al. (2020) developed a model-based estimation framework for pelagic false killer whales to generate spatially-explicit density estimates based on a habitat-based predictive density surface model (DSM). This DSM was the first developed specifically for pelagic false killer whales (i.e., excluded sightings attributed to insular populations) and provided density estimates at an approximate 9 km × 9 km grid resolution for the central Pacific during the summer-fall of 2002, 2010, and 2017, when the first three HICEAS efforts occurred.

The DSM captured distribution patterns that were consistent with previous model-based analyses of false killer whale distribution in the central North Pacific (Becker et al., 2012; Ferguson & Barlow, 2003; Forney et al., 2015), while improving upon those efforts. However, spatially-explicit measures of uncertainty in the density estimates were based on environmental variability during the prediction period and did not account for uncertainty in the density model parameters, detection parameters, or effective group size estimates (Bradford et al., 2020). In addition to recommending the incorporation of

additional sources of uncertainty into the model-based variance estimates, the authors identified several avenues for further development.

Following the most recent HICEAS in 2023 (Yano et al., 2025), we incorporated new survey data and recent technical and statistical advancements to improve the model-based estimation of Bradford et al. (2020) and herein provide updated abundance estimates of pelagic false killer whales in: 1) the full central Pacific study area, 2) the Hawai‘i pelagic false killer whale assessment area, and 3) the Hawaiian EEZ, for comparison to previous EEZ-based estimates. Methodological improvements include incorporating additional sources of uncertainty in variance estimation, statistically accounting for population ambiguity, and addressing extrapolation effects, as well as many other refinements. Additionally, we provide this updated methodology as a unified framework with modernized code and an accompanying vignette in a public repository for increased accessibility, transparency, and reproducibility to support the assessment and management of Hawai‘i pelagic false killer whales.

Methods

We used a model-based distance sampling analysis approach to estimate the density and abundance of pelagic false killer whales in the central Pacific, the Hawai‘i pelagic false killer whale assessment area, and the Hawaiian EEZ. With the exception of providing design-based estimates, which are not possible to obtain for the Hawai‘i pelagic false killer whale assessment area, we generally followed the approach of Bradford et al. (2020), with the following main improvements: variance propagation of detection and encounter rate parameters, a weighted-likelihood approach to address probabilistic stock assignments, and assessment of environmental extrapolation and associated use of clamping for out-of-bounds covariate values. Our DSM approach involved two stages: (1) the estimation of detectability parameters using distance sampling models, and (2) the estimation of density with an encounter rate model and group size model using generalized additive models (GAMs).

Through the two stages of the estimation framework, we used different partitions of a sightings dataset collected from 1986–2023 during ship-based line-transect surveys conducted throughout the central and eastern Pacific by SWFSC and PIFSC (Table 1). We used a larger subset of these data to estimate detectability parameters than was used for DSM building in the central Pacific. Sighting rates of false killer whales and other cetaceans in the central Pacific study area are low, partially due to an oligotrophic ecosystem that yields low densities of megafauna, but also due to difficult sighting conditions caused by predominant high sea states (e.g., Bradford et al., 2021). This data scarcity and lack of contrast across all detection conditions precluded robust estimation of detection parameters using sightings from line-transect surveys in this region alone. Therefore, we incorporated data collected from the eastern Pacific to estimate detectability parameters.

Data Collection

Ship Surveys

Our sighting data were collected during ship-based line-transect survey efforts led by SWFSC and PIFSC between 1986 and 2023 using consistent methods for distance sampling (Kinzey et al., 2000). The design and implementation of these surveys have been described extensively (e.g., Barlow, 2006; Bradford et al., 2014; Bradford et al., 2017; Bradford et al., 2020; Yano et al., 2018; Yano et al., 2025). In brief, the standard protocol for visual observations included a team of six observers who rotated through three positions on the flying bridge of the ship and searched for cetaceans forward of the vessel, from 90° left to 90° right. The port and starboard observers searched using

25x binoculars, while the center data recorder used their eyes or 7x binoculars. The observers remained on-effort while the ship traveled at 10 knots and the Beaufort sea state remained at 6 or below. When cetaceans were sighted, the observers recorded the initial bearing and radial distance to the sighting to compute the perpendicular distance from the trackline. When the sighting was within a strip width of 5.5 km (3 nmi) from the trackline, additional data collection steps took place so that species, species composition (for mixed-species groups), and group size could be estimated. The sightings used for estimation included both those made during systematic effort, i.e., when standard protocols were met while the ship was on an established design-based transect line, and nonsystematic effort, i.e., when standard protocols were met but the ship was not on designated transect lines.

False Killer Whale Sightings

The data collection protocol for false killer whale sightings has incrementally evolved in response to research efforts into their group behavior (Bradford et al., 2014; Bradford et al., 2020). Groups of false killer whales consist of multiple subgroups often spread out over tens of kilometers, with many subgroups beyond the transect strip width, creating a challenge for observers to accurately record group size (Bradford et al., 2014). However, accurately enumerating group size by accounting for individuals well outside the transect strip width would lead to positively biased estimates of abundance. Therefore, subgroup, rather than group, is a more appropriate unit of detection for line-transect data collection and analysis of false killer whales (Bradford et al., 2014).

For that reason, a two-phase subgroup-based data collection protocol (“PC” protocol) has been in place since 2011 for false killer whale sightings during ship-based surveys of the Pacific Islands region conducted by PIFSC. The first phase of the PC protocol allows on-effort observers the chance to detect and localize subgroups within the trackline strip width (to use in line-transect analysis), followed by a second phase where the ship approaches subgroups to obtain subgroup size estimates. Further information on the PC protocol is provided in Bradford et al. (2014), Bradford et al. (2020), and Yano et al. (2025). Following the PC protocol, weather and animal behavior permitting, the animals were approached by the ship, or a small boat launched from the ship, for further data collection to support individual and population identification.

Density Estimation

Study Area and Data Processing

The central Pacific study area of the DSM is defined as waters extending from the equator to 40°N and from 175°E to 132°W (Figure 1). Note this area was slightly truncated from the northern extent of 43°N used in Bradford et al. (2020), as environmental conditions at these northern latitudes were consistently outside of sampled ranges. The DSM dataset included all sighting and effort data collected during line-transect surveys conducted by SWFSC and PIFSC from 1997–2023 in the central Pacific (Table 1), with the majority collected more recently and within the Hawaiian EEZ (Figure 2). The additional sighting and effort data that informed the detection parameters used in the DSM were collected by SWFSC from 1986–2014 (Table 1) and extended beyond the central Pacific study area into the eastern Pacific (Figure 2). We only use effort data from surveys conducted outside of the central Pacific study area to estimate detectability parameters if that survey yielded a false killer whale sighting.

To create samples for modeling, we discretized continuous portions of on-effort survey tracklines using the R package *swfscDAS* (Woodman, 2025) with methodology described by Becker et al. (2010). Approximately 10-km segments were created to match the resolution of our environmental covariates. We used only on-effort data collected in Beaufort states 0–6 in the estimation, and chose a 5.5-km truncation distance based on previous analysis of large delphinid sightings (Barlow et al., 2011). All on-effort false killer whale sightings within a perpendicular distance of 5.5 km to the trackline were used to build the DSM and estimate detection parameters, including mixed-species sightings (though these are rare).

To ensure the DSM was specific to pelagic false killer whales in the central Pacific, we excluded sightings of the MHI insular and NWHI populations from the sightings dataset (Table 2). However, not all sightings in areas of population overlap around the Hawaiian Islands were able to be assigned to a population because relevant data (e.g., genetic samples) were not available. These sightings received a prorated pelagic assignment following Bradford et al. (2020). That is, we stochastically assigned the sighting to the Hawai‘i pelagic population with a probability equal to the prorated value. This prorated value was based on the proportion of Hawai‘i pelagic sightings represented after compiling relevant PIFSC and SWFSC ship-based false killer whale sightings of known population in the areas of population overlap around Hawai‘i.

Despite the transition to subgroup-based data collection and analysis, we were unable to use false killer whale subgroups as the modeling unit in the DSM without creating significant overdispersion, similar to Bradford et al. (2020). Thus, we used the approach

established in that analysis to generate “effective group sizes” (i.e., the total number of animals within all detected subgroups in a group), which both standardized the data across collection types and produced an appropriate group size measure for modeling. These effective group sizes were specified by the number of subgroups detected multiplied by the expected subgroup size (*E(s)*). We determined *E(s)* using the full set of consistently collected subgroup size estimates made on surveys since the implementation of the PC protocol. Before pooling estimates across protocol phases, we evaluated the effect of phase using the same generalized linear mixed modeling approach of Bradford et al. (2020), although the R package *glmmTMB* (Brooks et al., 2017) was used in the present analysis.

The actual number of detected subgroups during the first phase of the PC protocol was straightforward to extract for sightings made since 2011, when the protocol was implemented. However, sightings made before 2011 had to be standardized to the PC protocol in order to obtain an expected number of detected subgroups to compute the effective group size (see Bradford et al. 2020). This standardization treats each sighting as if the first phase of the PC protocol had occurred (i.e., as if the ship stayed on the trackline in passing mode). For sightings conducted using a group-size estimation protocol specific to HICEAS 2010, the expected number of detected subgroups was determined probabilistically using information from the observed subgroups relative to the projected trackline. For all other sightings, first the number of subgroups in the group was determined by dividing the estimate of total group size by *E(s)*, then the number of subgroups that were within the truncation distance was estimated, and finally the expected number of detected subgroups was determined using average subgroup detection probabilities.

Environmental Covariate Data

For the environmental predictors of density, we used outputs from the Global Ocean Physics Reanalysis product (GLORYS12V1), publicly available from the E.U. Copernicus Marine Service Information[2]. The GLORYS12V1 product is an ocean-eddy reanalysis with a spatial resolution of 1/12° at 50 standard levels. It assimilates in situ observations, satellite altimetry, sea surface temperature, and vertical profiles of temperature and salinity to provide 3D daily means of sea water potential temperature, sea water salinity, sea surface height, northward and eastward sea water velocity, and ocean mixed layer thickness, as well as sea ice variables.

[2] https://doi.org/10.48670/moi-00021

Note that Bradford et al. (2020) used the Hybrid Coordinate Ocean Model (HYCOM) as a source of environmental data, but GLORYS12V1 was selected over HYCOM in the updated analysis because it offers greater computational efficiency, faster download times, and a more user-friendly product that is regularly maintained. Its 0–360° grid is better suited for work in the Pacific Islands, and using GLORYS12V1 also ensures consistency with other PIFSC research efforts. We confirmed that both ocean models produce similar covariate values during the study period and thus did not expect switching from HYCOM to GLORYS12V1 for environmental data would affect the modeling results. From this product, we extracted sea surface height (SSH), mixed layer depth (MLD, designated as mixed layer thickness in the source data), and 0.5-m depth values for both potential sea surface temperature (SST) and salinity (SAL). These variables were then linked to the midpoints of on-effort segments in the DSM dataset. In addition to the four variables, we also calculated focal standard deviations (SD; within a 1 cell neighborhood of each focal cell) for each 9x9-km cell. High values of the focal SD are indicative of spatial fronts in the variable.

Model-based Approach

To develop a spatially-explicit assessment of pelagic false killer whale density across the study area, we followed the approach of Bradford et al. (2020) and Becker et al. (2016). We fitted two separate models: the first model was used to predict the encounter rate of false killer whale groups as a function of the environmental covariates, and the second model was used to estimate effective group size as a function of the environmental covariates. A separate group size and encounter rate model was chosen due to overdispersion when fitting a single-response model to this dataset.

Using the output of these two models and the standard line transect equation (Buckland et al., 2001), we modeled the density of pelagic false killer whales in a region along an approximately 10-km segment (indexed with *i*) of survey trackline using:

$$D_i = \frac{m_i}{g(0)_i \cdot ESA_i} S_i \qquad (1)$$

where m_i is a GAM-derived (Wood et al., 2017) estimate of the number of observed groups within the region; ESA_i is the effective search area of the region, which depends on detectability of the groups; $g(0)_i$ is the probability of detecting a group exactly on the survey trackline; and S_i is the GAM-based estimate of effective group size for groups within that region. In this analysis, we used modeled oceanographic variables as covariates in the group encounter rate and effective group size models (see description of the variables and models in the following sections).

Estimating the parameters and outputs for the DSM was accomplished in a two-stage process. First, we used distance sampling methods (Buckland et al. 2001) to estimate $ESA_i$and $g(0)_i$. In a second stage, spatially-explicit GAMs using ESA_i and $g(0)_i$ as offsets were fitted to model m_i and S_i components. After all DSM components were fitted, we estimated abundance estimates for regions of interest by partitioning the study area into regions (e.g., cells of a raster) and calculating:

$$N_R = \sum_{k \in R} D_k A_k \tag{2}$$

where R is the spatial region of interest, D_k is the density prediction for cell k in the region, and A_k is the area of the cell.

Detection Function

The perpendicular detection distances from the pooled central and eastern Pacific data were used to estimate parameters of a half-normal detection function (truncated at 5.5 km) using the R package *distance* (Miller et al., 2019). As in Bradford et al. (2020), we selected a half-normal detection function because it exhibits greater stability when fitting cetacean sighting data (Gerrodette & Forcada, 2005) and minimizes the effect of vessel attraction, which has been observed in false killer whales in the study area (Bradford et al., 2014). Beaufort sea state was used as a covariate in the model to account for variability in observation conditions (Bradford et al., 2020). From the fitted model, the effective search area (ESA) on each segment i can be estimated as:

$$ESA_i = 2 \cdot L_i \cdot ESW_i \tag{3}$$

where L_i is the known length of the segment, and ESW_i is the estimated effective strip width. The effective strip width is calculated as the integral (over distance) of the detection function and heuristically measures how far from the survey vessel observers are effectively able to detect animals given, in this case, sea state conditions. We calculated the Beaufort-specific ESW values for the pooled dataset to estimate the effective search area, ESA_i, used for density surface modeling with the central Pacific survey data. We also used the ESA values to estimate the Beaufort-based $g(0)_i$ values as described in the next section.

Trackline Detection Probability

To estimate the trackline detection probability, $g(0)_i$, on each segment i, we used the method of Barlow (2015) with the estimated ESA calculated as part of the detection function modeling. This method used the pooled central and eastern Pacific data to fit a

detection rate model and estimate a relative $g(0)$ value at each Beaufort sea state. For this portion of the analysis, all effort data within the central Pacific study area was used, but we only included effort data from surveys outside of the central Pacific if that survey had a sighting of false killer whales.

The relative $g(0)$ was measured relative to the ideal observation condition, Beaufort sea states 0–1, where we assumed $g(0)$ = 1. Following Barlow (2015), to fit the relative $g(0)$ model, hereafter referred to as $g(0)$, we used a GAM where the response was a binary indicator that false killer whales were detected on a segment of the pooled data. Covariates included Beaufort sea state as the key explanatory variable, along with year and spatial coordinates as nuisance variables. We used a shape constrained version of the GAM where the effect of Beaufort state was constrained to be monotonically decreasing. This ensured that predicted $g(0)$ values will decrease with increasing Beaufort sea state.

The probability (λ) of detecting a group on a survey transect i is assumed to be proportional to the area effectively searched, so the logarithm of the segment-specific ESA is included as an offset (Barlow et al., 2015). Following Barlow (2015), we used a Poisson distribution with the log rate:

$$\log \lambda_i = \log ESA_i + \beta_0 + f(b_i) + f(year_i) + f(x_i, y_i) \quad (4)$$

where β_0 is the intercept term; $f(b_i)$ is the effect on the detection rate for Beaufort state b = 0,...,6; $f(year_i)$ is a smooth year term; and $f(x_i, y_i)$ is a penalized spline function of the segment coordinates. To make sure that both Beaufort states 0 and 1 serve as the ideal condition, we set $f(0) = f(1)$. The model was fitted in the R package *scam* (Pya & Wood, 2015). To prevent model over-fitting, we limited the maximum degrees of freedom for the univariate terms (*year* and *Beaufort*; *scam* parameter *k* = 4), and the overall penalty for model complexity was inflated (*scam* parameter *gamma* = 1.4) (Barlow, 2015). Relative $g(0)$ values were estimated by calculating:

$$g(0; b) = \exp\{f(b)\} / \exp\{f(0)\} \quad (5)$$

for b = 0,...,6. For the DSM data set, $g(0; b_i)$ values were predicted for each segment based on observer-recorded Beaufort sea states. We used linear interpolation of the $g(0; b_i)$ in cases where sea state changed over the course of a segment.

We used a Monte Carlo approach to estimate the full covariance matrix of the detection function parameters and the $f(b)$ parameters, which was necessary for full variance propagation in the abundance estimates (see Variance Propagation subsection below). We used the Monte Carlo approach to account for the dependence between the detection function model parameters and the relative $g(0)$ model parameters because the relative $g(0)$ model used output from the detection function model. First, we

sampled 5,000 detection function parameter replications from its large sample distribution, $N(\theta_d, \boldsymbol{V_d})$, where θ_d are the estimated detection function parameters and $\boldsymbol{V}_d$ is the estimated covariance matrix. For each replication, we then calculated ESA for the pooled data segments and fit the scam model to estimate the $f(b)$ parameters, θ_g. The full estimated covariance matrix, $\boldsymbol{V}$, for $\theta = (\theta_d, \theta_g)$ was estimated with the empirical covariance matrix of the 5,000 θ samples.

Encounter Rate and Group Size Models

We fit the GAMs for encounter rate and effective group size using the R package *mgcv* (Wood, 2011). Effort and associated sightings from surveys outside of the central Pacific were excluded from this portion of the analysis. All sightings of pelagic false killer whales were included in the DSM dataset, including those with a probabilistic pelagic assignment. To account for these uncertain sightings in the model fitting process, we used a weighted likelihood approach where the weights were based on the assessed probability that the group belongs to the Hawai‘i pelagic population. The weighted approach was used because it accounts for added variance inflation (e.g., Alston et al. 2023) due to the uncertainty of the actual population identity of the sighting, as well as removing a potential negative bias when using a fixed discounted value for the number of groups and effective group size. For both of the GAM models, we used restricted maximum likelihood (REML) for parameter estimation.

Encounter Rate

For encounter rate, we modeled the number of groups sighted per segment (indexed by i) with a Tweedie family distribution, $TW(\mu_i, \varphi, p)$, where μ_i is the expected number of groups per segment, and φ and p are parameters that account for overdispersion and zero inflation in the group encounter rate. We use the Tweedie family as a general tool for cetacean modeling, as the Tweedie‘s index parameter p can provide flexibility to the variance structure to account for overdispersion or simplify to a more traditional Poisson distribution if overdispersion or zero-inflation are not present in the data (Miller et al., 2013). To model spatial density of groups, we must account for the area surveyed on each segment and the overall detectability of groups. Therefore, we used the effort variable:

$$\log E_i = \log g(0;\, b_i) + \log ESA_i \tag{6}$$

as an offset intercept in the GAM. Then, the expected number of encounters within a segment (m_i) is modeled relative to this effort:

$$\mu_i = E[m_i] = \exp\left\{\log E_i + \beta_0 + \sum_j f_j(x_{ij})\right\} \quad (7)$$

where β_0 is the intercept term, and the f_j term is a penalized spline function of the j^{th} environmental covariate.

To model the density of pelagic false killer whales, we must account for the sightings in areas of population overlap around the Hawaiian Islands with a prorated pelagic assignment. In Bradford et al. (2020), sightings with prorated pelagic assignments were handled by discounting the encounters and effective group sizes by the prorated value. Here, we take an alternative approach that reduces the influence of the sighting based on the assessed probability, w_i, that the sighting was a pelagic group. Instead of using a fixed and discounted encounter value for a given sighting, we used both possible values (m_i or 0) depending on whether the sighting was a pelagic group or not. Each value's contribution to the likelihood is weighted by the probability the sighting is pelagic:

$$\log L(\beta_E, \varphi, p|\boldsymbol{m}, \boldsymbol{w}) = \sum_i w_i \log TW(m_i;\ \mu_i, \varphi, p) + (1 - w_i) \log TW(0;\ \mu_i, \varphi, p) \quad (8)$$

where w_i is the assessed probability that the sighting was a pelagic group and β_E are the encounter rate model parameters. If there was no sighting (m_i = 0) in a segment, then w_i = 1.

To fit this weighted model, for each m_i > 0, we augment an identical row to the encounter data set with m_i = 0. This approach is an example of a relevance weighted likelihood (RWL; Hu & Zidek, 2002). The RWL allows inclusion of other data which may have relevance to parameter estimation, with the analyst deciding how relevant based on the weight assigned (Wang, 2001). In this case, every segment has two datums, the observed m_i and 0. We use the w_i to adjust the relevance of each value to the likelihood. The total level of information in the augmented data remains the same as the unweighted version because the sum of the weights is still equal to the number of surveyed segments. Wang (2001) notes that RWL fit models can have improved mean-square error properties in many instances.

An alternative to the weighted likelihood approach is a stochastic imputation approach (e.g., Hanks & Hughes, 2016), where we would randomly select an indicator of inclusion based on w_i, fit the model in the traditional unweighted fashion, and repeat many times. However, this approach would be too computationally demanding to implement in the variance propagation and model selection stages. We chose the weighted approach because it can easily be implemented in all stages of the estimation via the *mgcv* package.

Variance Propagation

One criticism of the 2-stage DSM framework has been that uncertainty in the effort offset, $\log E_i$, is not usually propagated correctly into the final variance estimates of density predictions from the GAM models (Bravington et al. 2021). In previous DSMs for this population, including Bradford et al. (2020), multiple sources of uncertainty (environmental variability, detection parameter estimation, and effective group size estimation) were quantified and combined using the delta method to provide an overall measure of variance for the model-based estimates. Here, we incorporated recent developments to quantify spatially-explicit variance that account for combined sources of uncertainty in abundance prediction. Specifically, for the encounter rate model, we used the approximation method developed by Bravington et al. (2021), who show how to reformulate the DSM so that the uncertainty in $\log E_i$ from the distance sampling stage is captured as an extra random effect in the encounter rate model. The extended model for more accurate parameter variance inference is:

$$\mu_i = E[m_i] = \exp\left\{\log E_i(\theta) + \frac{\partial \log E_i(\theta)}{\partial \theta}\nu + \beta_0 + \sum_j f_j(x_{ij})\right\} \quad (9)$$

where $\theta = (\theta_d, \theta_g)$ is a vector of the detection function and $g(0; b)$ parameter estimates from the first stage, ν is a multivariate random effect with distribution $\nu \sim N(0, \boldsymbol{V}), and\ \boldsymbol{V}$ is the covariance matrix of θ estimated with the Monte Carlo simulation described previously. We used functions within the R package *dsm* (Miller 2025), which contains a modified version of the *mgcv* `gam()` function, to fit this model when assessing spatial uncertainty of the regional abundance estimation. The same weighted likelihood was used to fit the extended model.

Group Size

The response variable of the group size model was derived effective group sizes, S_k, reflecting the total number of animals within all detected subgroups for each sighting k. The group size model was fit to the natural logarithm of effective group sizes with a Gaussian link function. The mean function form used for sighting k was:

$$\mu_k = E[\log(S_k)] = \beta_0 + \sum_j f_j(x_{kj}) \quad (10)$$

where, as with the encounter rate model, $f_j(x_{kj})$ are penalized spline functions of the environmental covariates. Because we condition on sighting a group for these data, there is no detection effort offset for this model. As with the encounter rate model, to adjust for the possibility that a sighting was not of a pelagic group, we used a weighted

likelihood function for estimation. The weighted log (REML) likelihood for the group size analysis was:

$$\log L(\beta_G, \sigma^2 | \boldsymbol{S}, \boldsymbol{w}) = \sum_i w_i \ \log N(\log S_i;\ \mu_i, \sigma^2) \tag{11}$$

where w_i is the assessed probability that the sighting was a pelagic group, and β_G are the parameters for the group size mean function. Here, likelihood is not evaluated at zero with weight 1-w_i as in the encounter rate model because if the group is not pelagic, it would not be included in the analysis. So, the relevance of the likelihood component contribution is down weighted by any w_i < 1. For abundance prediction, we used the predicted group size for each day and cell, which is calculated as:

$$\widehat{S_j} = \exp\{\widehat{\mu_j} + 0.5\sigma_j^2\} \tag{12}$$

where j indexes a particular day and cell. The additional variance term accounts for the bias induced by back-transforming the predicted log group size.

Model Selection

In order to select parsimonious models for encounter rate and effective group size, we used the Akaike information criterion (AIC, Akaike, 1973) to select from a suite of models. For encounter rate, each of the raw environmental variables, SST, SSH, MLD, and SAL, could be included along with the focal variance versions (SST_SD, SSH_SD, MLD_SD, and SAL_SD) for a total of eight considered covariates within each model. In addition to the set formed from all combinations of the 8 covariates, as in Bradford et. al (2020), we allowed for the possibility that one of the four main covariates might interact with latitude, such that the covariate effect varied on a latitudinal gradient. In this way, a tensor product smooth of the covariate and latitude was substituted for the spline function of the covariate on its own. Thus, the tensor product smooth served as an interaction term, where the association between animal density and the covariate was mediated by latitude and accounted for situations where the covariate is correlated with latitude, such as temperature. The full suite of considered encounter rate models was composed of 767 models. Due to the limited number of sightings for the group size model, we examined a model suite of all possible combinations of only the four main covariates for a suite of 16 models.

In both models, REML was used to estimate parameters (Marra & Wood, 2011). In addition to elimination of variables in model construction, the *mgcv* `ts` smoothing spline was used, which allowed the smooth to be identically zero and removed from the model as part of the fitting process (Marra & Wood, 2011). Finally, to avoid overfitting, the top

AIC models were examined, and any variables that had *p*-values ≥ 0.05 were also removed; models were then refit to ensure that all remaining variables had *p*-values < 0.05 (Redfern et al. 2017, Roberts et al. 2016).

Model Validation

Traditional cross-validation is not possible for this analysis due to limited data availability to discretize into training and testing datasets. For this rare taxon, our results may be particularly sensitive to each data collection effort, especially the more extensive HICEAS surveys. We computed retrospective estimates to assess this sensitivity, where we refit the final model, sequentially leaving out each HICEAS effort (2002, 2010, 2017, and 2023) in each fold, and then examined the variation across folds in predicted abundance estimates for the final estimation year. Variance propagation was not performed on folds to ease computational demand, and as such, estimated confidence intervals should not be compared to the confidence intervals of the final abundance estimates.

Model performance was further evaluated using established metrics outlined in Bradford et al. (2020), including the percentage of explained deviance, the area under the receiver operating characteristic curve (AUC, Fawcett, 2006), the true skill statistic (TSS, Allouche et al., 2006), and the ratio of average observed density to predicted density in the central Pacific region. AUC and TSS metrics are used to evaluate presence predictions, not density per se. However, pelagic false killer whales are so sparsely detected that predicting presence is very similar to density. In addition to the model validation metrics used in Bradford et al. (2020), we also used the random over-sampling examples (ROSE) sampling bootstrap (Lunardon et al. 2014) to determine the effects that the sparse detection of false killer whales might have had on AUC and TSS metrics.

AUC discriminates between true-positive and false-positive rates, and values range from 0 to 1, where a score of > 0.5 indicates better than random discrimination. TSS accounts for both omission and commission errors and ranges from -1 to 1, where 1 indicates perfect agreement and values of zero or less indicate performance no better (or worse) than random. To calculate TSS, the ROC plot-based approach (Liu et al., 2005) was used to obtain a threshold for false killer whale presence. We calculated the AUC and TSS from the fitted DSM models as in Bradford (2020). Menardi and Torelli (2014) note that when data are highly imbalanced, performance metrics such as AUC or TSS can be compromised.

Due to the sparsity of encounters, we also included the ROSE sampling bootstrap to assess the value of the covariates used in the encounter rate model as predictors of

encounters. The ROSE sampling method is described in detail by Menardi and Torelli (2014), but briefly, kernel density estimates (KDEs) are calculated for segments with and without detections. Then a sample is drawn with probability = 0.5 from each KDE until the desired sample size is reached. This process produces a balanced sample where the predictive covariates are similar to what was observed for each group (detection vs. nondetection) in the original data. The ROSE resampling bootstrap predictive assessment algorithm proceeds as follows (Lunardon et al. 2014):

1. For original data D_n, obtain a ROSE sample of size m, R_m, that balances the number of segments with detected groups and no detected groups. We used m = n.

2. Fit the GAM model with R_m and make predictions for the original data. For predictions, we used the probability that the number of groups on a segment was greater than zero. For a Tweedie distribution this is:

$$p_i = 1 - exp\left\{-\frac{\mu_i^{2-p}}{1+\varphi(2-p)}\right\}. \quad (13)$$

3. Compute AUC and TSS relative to original data, D_n.

4. Repeat *B* times (we used *B* = 50).

We examined the distribution of the ROSE performance statistics relative to the ones calculated using only the original, unbalanced data. The R package ROSE (Lunardon et al., 2014) was used to perform the balancing bootstrap.

In addition to model performance where data are observed, determining areas where model predictions may break down is also an important aspect of model validation. Our model building dataset has excellent spatial coverage within the Hawaiian EEZ, but it has very limited coverage in the rest of the central Pacific, where these predictions are made (Figure 2). To assess whether applying our results to unsampled regions was appropriate, we compared the range of environmental conditions in the DSM model building datasets to our predicted locations using the methods outlined by Bouchet et al. (2020) for both univariate and multivariate characterizations. If there were areas within the central Pacific study area where extrapolation conditions occurred within the dates of prediction, we truncated all oceanographic variable values to be ≥ 0.1 and ≤ 99.9 percentiles of the oceanographic variables that were observed on the dates and locations of the survey segments. Such clamping ameliorates the effects of extrapolation outside of the conditions with which the DSM models are built and selected (Bouchet et al. 2019).

Finally, we used a Bayesian posterior predictive diagnostic to assess whether the fitted model can produce replicated data metrics that are similar to the same metrics calculated from the observed data (Conn et al. 2018). Specifically, we simulated 200 parameter replications from the posterior distribution of the encounter rate and group size models using importance sampling. For each replicate, we used the fitted model to draw encounter data from the Tweedie distribution and group sizes from the log-normal distribution for each encounter > 0. For each replicated data set we calculated the number of positive encounters and the posterior predictive average density (number of replicated sightings divided by total ESA) over the central Pacific region. These posterior predictive quantities were compared to the observed number of effective detections (n_{eff} = w_i) and empirical density (n_{eff} divided by total ESA) to look for large model deviations.

Abundance Estimation

The relationship between the habitat covariates and the encounter rate and group size models were used to predict spatially-explicit density values for the full central Pacific study area during 2017 and each year from 2020 to 2024. The 2020–2024 period represents the most recent five-year period at the time of analysis and encompasses the years of new survey data (2020, 2023; Table 2) since Bradford et al. (2020). Estimating abundance in 2017 was used primarily as a point of comparison with Bradford et al. (2020). Similar to Bradford et al. (2020), we generated model predictions for separate tri-daily (3 sequential days) environmental conditions covering July 1 to December 31 of each year. The 6-month window was chosen because it covers each of the HICEAS effort periods (2002, 2010, 2017, and 2023). These tri-daily predictions were then averaged within each year to produce spatial grids (1/12° resolution) of average pelagic false killer whale density within the central Pacific for each year. We also computed a multi-year average of all predicted tri-daily false killer whale densities from 2020–2024 to account for varying oceanographic conditions during this period.

We estimated the abundance of pelagic false killer whales in each region (central Pacific, Hawai‘i pelagic false killer whale assessment area, and Hawaiian EEZ; Figure 1) as the sum of the individual grid cell abundance estimates, which were derived by multiplying the cell area, within the region in question, by the predicted cell density, exclusive of any portions of the cell located on land. For the density point estimates, the original encounter rate model with a fixed log effort offset was used to predict density for each raster. Area calculations were completed using R package *terra* (Hijmans, 2025).

Uncertainty from all model components (detection, encounter rate, and group size) was propagated to the final abundance estimates through a posterior simulation approach (also known as parametric bootstrapping, Miller et al., 2022). The uncertainty procedure we used is as follows:

1. Fit the extended encounter rate model (with Jacobian random effect term) (Bravington et al., 2021). Sample 200 parameter values from the posterior distribution of the extended encounter rate model using importance sampling (Givens & Hoeting, 2012).
2. Sample 200 parameter values from the group size model using importance sampling.
3. For every third day (tri-daily, for computational efficiency) from July 1 to December 31 in the years 2017, 2020–2024, calculate 200 abundance estimates with each GAM parameter sample. There were 74,400 total abundance predictions for each region of interest, 200 parameter replications, 62 days, and 6 years.
4. For a region and time span of interest, calculate the coefficient of variation (CV) with:

$$CV_{Rt} = \frac{\mathrm{sd}\left(N_{Rjd}\right)}{\mathrm{mean}\left(N_{Rjd}\right)} \tag{14}$$

where N_{Rjd} is the abundance estimate for the j^{th} parameter replicate for date d in region R. The sd( ) and mean( ) summaries are for the dates within the time span of interest, e.g., 2017 or 2020–2024.

Step 1 allowed us to account for the detection parameter and encounter rate model parameter uncertainty in the abundance estimates. Step 2 allowed us to account for the group size model parameter uncertainty. Finally, step 3 allowed us to account for temporal variability in environmental conditions during the survey period. After calculating the CVs for regional abundance estimates, we used a lognormal approximation to calculate confidence intervals (CI) for each estimate using the form:

$$95\%\, CI = \exp\{\mu \pm 1.96\sigma\} \tag{15}$$

where $\mu = \log(N) - \sigma^2/2$, $\sigma^2 = \log(1 + CV^2)$, N is the abundance estimate, and CV is the coefficient of variation calculated in step 4.

Results

Survey Sightings

Data from 135 false killer whale sightings collected on 40 ship-based line-transect surveys from 1986 to 2023 (Table 1, Figure 2) were used to derive the detectability parameters, $g(0)$ and ESW (Table 3). Our habitat-based density model was fit to a subset of these data, which included a total of 14,399 10-km survey segments from 20 line-transect surveys conducted from 1997–2023 within Beaufort sea state conditions 0–6. These efforts yielded 44 pelagic or possibly pelagic false killer whale sightings, 35 of which were observed during systematic survey effort (Table 2, Figure 3).

The majority of sightings were confirmed to be pelagic false killer whales using photo-identification, genetic, telemetry, or location inference, but 13 were probabilistic pelagic assignments, with 8 sightings overlapping with the range of the MHI insular false killer whale population and 5 overlapping with the range of the NWHI population (Table 2). Based on the compiled ship-based false killer whale sightings of known population in the area where the MHI and Hawai‘i pelagic populations overlap (n = 11 sightings between 2005 and 2017) and the NWHI and Hawai‘i pelagic populations overlap (n = 5 sightings between 2010 and 2017), the 8 MHI or Hawai‘i pelagic sightings were assigned a pelagic probability of 0.18, and the 5 NWHI or Hawai‘i pelagic sightings were assigned a pelagic probability of 0.6. The effective number of pelagic detections in terms of likelihood weighting is equal to the sum of the probabilities that each of the 44 sightings represent pelagic false killer whales, n_{eff} = 35.45.

Finally, 151 false killer whale subgroup size estimates collected between 2011 and 2023 using the PC protocol were determined not to differ by phase (n = 74 phase 1, n = 77 phase 2; predictor coefficient estimate = 0.08, Wald z = 0.67, p-value = 0.51). Thus, the subgroup size estimates were pooled, producing an $E(s)$ of 2.26 (SD = 1.62) that was multiplied by the actual or expected number of subgroups to obtain an effective group size for each DSM sighting (Table 2).

Model Components

Detection Components

Using all 135 sightings in the augmented surveys, a half-normal detection function with a Beaufort-specific range parameter was estimated (Figure 4). The range parameter of the detection function declined significantly with Beaufort sea state conditions (b = 0,...,6), with a log linear slope of -0.13 [95% CI: -0.03–0.23], resulting in Beaufort-

specific ESW and $g(0)$ values that also decrease with increasing Beaufort state (Table 3).

GAM Models

An evaluation of the 767 encounter rate models revealed that all 128 models that included the SST/Latitude tensor smooth were the top models, however, there was very little difference between the top 128 models (ΔAIC < 2). Collectively, they accounted for 60% of the total Akaike model weight, a substantial proportion for the SST/Latitude interaction term. We examined the top AIC model: (SST/Lat) + SSH + SSH_SD + SAL_SD and determined that only the (SST/Lat) tensor product term was significant (Appendix A). Therefore, following Bradford et al. (2020), we removed the insignificant terms and used a model containing only the (SST\Lat) term for density prediction, which explained 4.9% of the overall deviance (Appendix A). Generally, expected group density increases southward as SST increases (Figure 5). The index parameter *p* of the Tweedie distribution was 1.01, strongly tending toward a Poisson distribution, reflecting a low incidence of overdispersion in the data.

The top AIC model for effective group size contained the terms SSH and MLD, with a percent deviance explained of 28.7% (Appendix A). All terms were significant in this model, so they were retained for prediction in the study area. Expected effective group size increases with increasing SSH and decreases with increasing MLD (Figure 6).

Model Validation

The abundance estimates of pelagic false killer whales in 2024 resulting from the retrospective estimate exercise showed moderate variation, with estimates for the Hawaiian EEZ showing greater variation than estimates for the Hawai‘i pelagic false killer whale assessment area or central Pacific study area (Table 4). The ratio of the empirical density to DSM model-predicted average density (1.06) throughout the central Pacific region did not provide evidence of systematic bias in the model-based estimates. The observed density is 0.093 per 100 km^2 and the 95% credible interval for the posterior predictive average density is [0.047–0.137]. In addition, the predicted number of encounters is 35.73 [21–52], similar to the observed effective number of encounters of 35.45, suggesting the fitted models are able to produce detections at similar overall rates to what was observed.

The traditional prediction assessment statistics for the current model predictions are AUC = 0.71 and TSS = 0.36, while the ROSE sample corrected prediction assessments are AUC = 0.76 (range 0.758–0.767) and TSS = 0.43 (range: 0.41–0.45), both

indicating better than random performance. While the ROSE values are larger than the original versions, as expected due to imbalance correction, they are very similar, suggesting that the sparsity of the data is not dramatically affecting prediction assessment.

In the heuristic assessment of prediction extrapolation, ocean conditions in the Hawai‘i pelagic false killer whale assessment area and the Hawaiian EEZ were generally similar to those used to fit the model (Figure 7). The majority of the assessment area was not subject to extrapolation as characterized by the methods of Bouchet et al. (2020). However, environmental conditions in the southern reaches of the central Pacific study area, specifically in 2023, were consistently outside of the ranges of the environmental data in the DSM data sets.

The proportion of days experiencing extrapolation conditions is low on average throughout the EEZ (0.17%) and assessment area (0.19%). Therefore, we have a reasonable level of confidence that the model structure remains sound for prediction in these regions, and density estimates should not be unduly affected by extrapolation issues. However, the southwest region of the greater central Pacific study area can experience extrapolation conditions, with some areas experiencing extrapolation conditions over a high proportion of the prediction days (Figure 7). The average proportion of extrapolation conditions in the central Pacific as a whole is 4.5%. This effect is especially notable in 2023 (11.2% average proportion). Therefore, covariate clamping was used so that the extrapolation conditions would not lead to unreasonable density predictions.

Abundance Estimates

For 2020–2024, the average pelagic false killer whale abundance in the central Pacific study area was 33,216 [95% CI = 9,917–82,950] individuals, equivalent to a density of 0.13 [95% CI = 0.04–0.33] individuals per 100 km^2 (Table 5, Figure 8). In the Hawai‘i pelagic false killer whale assessment area, the 2020–2024 abundance was 4,526 [1,547–10,444] individuals, with an associated density of 0.07 [95% CI = 0.02–0.15] individuals per 100 km^2 (Table 5, Figure 9). Finally, for the Hawaiian EEZ, the 2020–2024 abundance was 1,745 [526–4,334] individuals, with a density of 0.07 [95% CI = 0.02–0.17] individuals per 100 km^2 (Table 5, Figure 9).

Yearly estimates are similar to these averages (Table 5), with the exception of the 2023 central Pacific estimate, which is substantially higher due to the warmer conditions in the southwest of the region (Figure 8).

Using the updated DSM, estimates for average abundance in 2017 (Table 5, Figure 8, Figure 9), are generally smaller, but of similar magnitude, to the central Pacific and Hawaiian EEZ estimates from Bradford et al. (2020) and the assessment area estimate from Oleson et al. (2023). Specifically, the 2017 estimates are 6% smaller for the central Pacific study area, 16% smaller for the Hawai‘i pelagic false killer whale assessment area, and 12% smaller for the Hawaiian EEZ. However, the central Pacific difference may be larger than it appears because the current estimates are for a slightly smaller study area. The updated 2017 estimates are all well within the CIs of the corresponding estimates from Bradford et al. (2020) and Oleson et al. (2023), so there is no statistically significant difference between them. After removing the 2020 and 2023 survey data, as well as data from one survey in 2010 not used in the Bradford et al. (2020) DSM, we obtained 2017 abundance point estimates of 5,335 and 2,268, respectively, for the Hawai‘i pelagic false killer whale assessment area and the Hawaiian EEZ. These estimates are 3% smaller and 9% larger, respectively, than the original estimates but also well within the CIs.

In general, the updated spatial distribution patterns of abundance (Figure 8) match those observed by Bradford et al. (2020). Most of the predicted abundance exists in the southern portion of the central Pacific study area, the bulk of which occurs in the west, with a band stretching to the east outside of the Hawai‘i pelagic false killer whale assessment area. Spatial distribution in the Hawaiian EEZ shows higher predicted abundance on the western side of the EEZ and additional high spots west of Hawai‘i Island (Figure 9). After accounting for detection parameter uncertainty, DSM (GAM) parameter uncertainty, and temporal variation in oceanographic conditions, the uncertainty in predicted abundance is very large at the extreme ends of the central Pacific study area (Figure 10). This uncertainty was not unexpected and was the main reason for removing the top 3° of latitude from the northern end of the study area defined in Bradford et al. (2020). The estimated CV was <1.0 for the vast majority of the Hawai‘i pelagic false killer whale assessment area and the Hawaiian EEZ (Figure 11), with the majority of the spatial uncertainty in the western and northern sides.

Discussion

In the present study, we provide abundance estimates of pelagic false killer whales in the central Pacific, the Hawai‘i pelagic false killer whale assessment area, and the Hawaiian EEZ using an updated estimation framework and the most comprehensive line-transect survey dataset available to date. While this effort largely follows the approach of Bradford et al. (2020), our improvements provide a more statistically robust analysis and an accessible and reproducible workflow.

The most supported model for group encounter rate indicates that encounters increase with temperature on a latitudinal gradient, where lower latitudes (and correlated higher temperatures) were associated with a greater encounter rate (Figure 5). Effective group sizes were best modeled using additive effects of sea surface height and mixed layer depth, with larger groups being associated with larger heights and shallower mixed layer depths (Figure 6). Sea surface height provides an indication of mesoscale features such as eddies and fronts (Chelton et al., 2011), and together with shallower mixed-layer depths, may indicate more productive areas to support larger groups.

Similar to previous habitat models developed for false killer whales in the central North Pacific (Becker et al., 2012; Forney et al., 2015; Bradford et al., 2020), the highest predicted densities occur near the equator, and the lowest predicted densities in the northeastern portion of the study area (Figure 8). Though estimated abundance for the assessment area and EEZ were relatively consistent over the study period (Table 5), the estimated abundance of pelagic false killer whales in the central Pacific was notably high in 2023, an apparent outlier year likely associated with a strong El Niño and accompanying warmer sea surface temperatures (Geng et al., 2024). In predicting false killer whale density across the central Pacific study area and specific regions therein, the warmer southern regions were subject to our clamping approach (Figure 7) to avoid extrapolating our functional curves past sampled conditions.

Influence of Additional Survey Data

Our approach yielded abundance estimates from 2017 that are smaller to varying degrees than the central Pacific and Hawaiian EEZ estimates reported in Bradford et al. (2020) and the Hawai‘i pelagic false killer assessment area estimate reported in Oleson et al. (2023). However, the estimates resulting from running the updated DSM with the Bradford et al. (2020) dataset are more closely aligned, suggesting that differences between estimates here and in the Bradford et al. (2020) analysis are primarily driven by a reduction in encounter rate in the additional data collected since 2017.

Specifically, there was a rate of 1.5 effective pelagic false killer whale detections per 1000 survey segments in the new data additions compared to 2.7 effective detections per 1000 survey segments in the data used by Bradford et al. (2020). Surveys conducted since 2017 have increased the overall effort available for modeling by roughly 20%, with only a 9% increase in false killer whale sightings. These survey efforts include a winter survey (Yano et al. 2020) and a summer-fall survey during the strong El Niño of 2023 (Yano et al. 2025). Reduced encounter rates in recent years could be attributed to differences in environmental conditions that influence detectability or shifts in animal distribution, including to outside of the sampled area. The average Beaufort sea states experienced in surveys in 2020 and 2023 are significantly higher than those during prior surveys used in the DSM (4.4 and 4.0, respectively; $t = 6.296$, p-value < 0.001).

The retrospective estimates showed the greatest change in predicted abundance, but relatively smaller 95% confidence intervals, when the data from 2017 were omitted. 2017 was a survey year with a relatively high encounter rate and relatively cooler La Niña conditions (i.e., 2010), suggesting that pelagic false killer whale distribution is influenced by local conditions and that shifts throughout or outside of the study area are important to consider.

Further, the inclusion of these additional data and our updated workflow supported a different functional form to describe variation in encounter rate and effective group size. The false killer whale densities in Bradford et al. (2020) were predicted using sea surface temperature, the standard deviation of sea surface temperature, and the tensor smooth of sea surface height and latitude for encounter rate and mixed layer depth for group size. With additional data, a positive effect of sea surface height also became significant in the group size model, and the percent deviance explained is a little over twice as large as the group size model from Bradford et al. (2020).

Influence of Methodological Changes

The present analysis incorporated several methodological changes from the approach described in Bradford et al. (2020), while retaining the same basic model structure. First, we propagated uncertainty from all estimated parameters in the encounter rate model, including ESA and $g(0)$ in the offset intercept, into the spatially-explicit abundance estimates, leading to larger variances. Variance propagation in DSMs is a relatively new method (Miller et al. 2022), and was not available at the time of Bradford et al. (2020). More recent DSMs for other cetacean species in the Hawaiian EEZ have used variance propagation, though not for the entire offset intercept. Becker et al. (2022) estimated spatially-explicit measures of variance that accounted for environmental variability and uncertainty in the GAM parameters and ESW, but they

were unable to apply uncertainty in $g(0)$ to pixel-specific predictions, as the variance propagation method developed by Miller et al. (2022) was not suitable for segment-specific $g(0)$ estimates.

Second, we improved the method of incorporating sightings with probabilistic assignment to the Hawai‘i pelagic stock for those sightings in areas of stock overlap. In Bradford et al. (2020), all pelagic or possibly pelagic sightings were used for the encounter rate and group size model, but the encounter rate, and thus effective group sizes, were weighted by the probability the sighting was part of the Hawai‘i pelagic population. While this method did address the uncertainty in population assignment, the resulting average effective group sizes were likely biased low and overdispersed. Our updated method incorporates the probability of an encountered group being pelagic into the likelihood weighting, a more statistically robust method that lends greater accuracy and precision.

Finally, we addressed extrapolation through not only truncating our study area to a region where environmental conditions are consistently within sampled ranges, but also by clamping the habitat response curves. As our encounter rate model results showed increasing and linear covariate functional curves, clamping the response is the more reasonable method of environmental extrapolation than allowing an unconstrained response curve or fully truncating out-of-bounds pixels (Guevara et al., 2018; Bouchet et al., 2019; Becker et al., 2025). This method is preferred over truncation, where model predictions made outside of the multivariate space of the data used to develop the models are discarded, as eliminating spatially or temporally clustered pixels can bias final averages.

Model Performance

There were insufficient sighting data to carry out traditional model validation using a testing and training dataset, a limitation of the Bradford et al. (2020) estimation that was not resolved with data collected since 2017. Instead, we implemented multiple methods to assess our model, such as posterior predictive checking and retrospective estimates leaving out each HICEAS survey, among other model performance metrics.

Our posterior predictive checks did not show systematic discrepancies between observed data and data predicted from our final model. In predicting abundance from our final model fit with different partitions of the data, we found moderate variation in estimated abundances, but no indications that one survey is substantially influencing results over the entirety of the central Pacific (Table 4). However, each survey is influential when considering abundance within the Hawai‘i pelagic false killer whale assessment area or Hawaiian EEZ, revealing the importance of surveying across the

broad set of habitat relationships (Table 4). When removing the survey conducted during the strong El Niño of 2023, we estimated lower abundance in 2024 for the central Pacific compared to the model fit to the full dataset, but larger abundances in the assessment area and EEZ. Removing the survey from 2010, which coincided with a strong La Niña, had the opposite effect, resulting in higher central Pacific abundance in 2024 but lower assessment area and EEZ abundance. More pelagic false killer whale sightings were made during HICEAS 2010 than HICEAS 2023, so this discrepancy may reflect a higher pelagic false killer whale density close to the Hawaiian Islands with cooler sea-surface temperatures. This result underscores the continuing need for large-scale surveys to understand habitat relationships in a dynamic ecosystem.

Our models showed better than random performance using three metrics (AUC, TSS, and ROSE). We also addressed extrapolation in projecting our DSM onto novel environmental space by clamping those response curves within 0.1% of observed covariate range, which improved the reliability of our results. Our approach provides better-informed interpretations of model output and associated uncertainties by avoiding biases in abundance estimates stemming from fluctuations in environmental conditions outside of sampled regions. For example, in 2023, the unsampled southern reaches of the study area were extremely warm, which, without clamping, would have resulted in very high predicted encounter rates due to the model-estimated relationship between encounter rate and the multivariate smooth of sea surface temperature and latitude. While density surface models would ideally be developed using data collected from the entire region of interest, the broad range of pelagic false killer whales in the central Pacific makes such surveys logistically and financially infeasible.

Model Assumptions and Limitations

We estimated trackline detection probability ($g(0)$) relative to ideal sighting conditions, where at a 0 or 1 Beaufort sea state, $g(0)$ is assumed to be 1. Trackline detection probability can also be affected by availability of animals to sampling, e.g., during diving or when exhibiting cryptic surface behavior (Rankin et al., 2020). Because false killer whales are highly surface active and often travel in spread out groups, we suggest that variation in $g(0)$ due to sighting conditions is much larger than variation due to animal behavior over the course of an encounter. However, the relative $g(0)$ estimates presented here may still be biased and could instead be used to scale $g(0)$ values in future analyses should estimates of availability be obtained.

Our approach also makes the assumption that true group densities are independent of sea state, which would be violated if false killer whales in our study were more likely to occur in windy or calm areas. However, as noted in Barlow (2015), the geographic terms in $g(0)$ should capture the effect of correlation between animal density and broad-

scale variation in sea state, and the Beaufort term should capture effects of day-to-day (and sometimes hour-to-hour) variation in sea state. In practice, Beaufort sea state is an empirical tool to account for factors affecting visibility that cannot be predicted for areas or time periods outside of surveys. Thus, it would be challenging to incorporate Beaufort as a covariate in the density estimation.

There are still some sources of uncertainty in our modeling framework that remain unaccounted for in our variance propagation approach, such as covariate uncertainty (resulting from measurement error), smoothing uncertainty (choice of basis functions and size), model selection uncertainty, uncertainty from deriving effective group sizes, and uncertainty in our pelagic proration in the weighted likelihood. Additionally, the posterior simulation approach used to account for uncertainty in group size in the abundance estimates did not account for covariance between our group size and encounter rate models. While it is likely that encounter rate and group size are largely independent, our environmental covariates are likely correlated. Future iterations of this model should consider a Bayesian formulation to more naturally incorporate uncertainty from the auxiliary analyses used to derive effective group sizes and pelagic proration values (for more details on these analyses, see Bradford et al. 2020), as well as covariation among component models.

In terms of model selection uncertainty, we exhaustively tested over 700 encounter rate models in our model selection procedure, and found that the vast majority of those models had very similar out-of-sample predictive accuracy (as measured by AIC) and percent deviance explained (see Table B1 for examples). The top 4 group size models had nearly identical AIC values and percent deviance explained (Table B2), and after removing nonsignificant terms were also identical, with sea surface height and mixed layer depth as covariates. To test the sensitivity of the final abundance estimates to uncertainty in model selection, we predicted abundance from various encounter rate models with similar AIC values and percent deviance explained (Appendix B). We found that final abundance estimates among these models are, similarly, quite close (Table B3), so our results are robust to uncertainty in model selection.

The lack of differentiation in AIC among encounter rate models and relatively low percent deviance explained by the most supported encounter rate model (4.9%) indicates a lack of information in this sparse pelagic false killer whale dataset for determining where groups occur. The top-ranked model for encounter rate (before non-statistically significant terms were removed) included sea surface height, the standard deviation of sea surface height, and salinity, as well as the interaction term between sea surface temperature and latitude, and still only explained 5.9% of the deviance (Table B1). The low deviance explained may be attributed to the low number of encounters providing little power to predict habitat relationships. Additionally, spatially, false killer whale groups occur across the entire central Pacific study area (Figure 3), and there

ultimately may not be sufficient contrast in the suite of tested covariates to determine false killer whale habitat preferences with precision.

It is likely that this entire region is appropriate habitat for false killer whales, and given that this population is relatively rare and highly mobile, it will be perpetually challenging to build a DSM that explains a large percentage of deviance. Further, we may have likely omitted important covariates that govern false killer whale space use. We did attempt to include biological variables in model formulations (Appendix C), but their associated parameters were not supported for inclusion in the final model for either encounter rate or group size ($p > 0.05$). There are potentially other covariates that could be included to improve model performance, such as prey information. However, these covariates would need to be available (or able to be predicted) at a very fine spatiotemporal resolution across a vast remote region to be used in predicting abundance across our study area.

In predicting pelagic false killer whale abundance in different spatial regions and at different temporal scales, we made the implicit assumption that habitat associations do not vary over space and time (Mannocci et al., 2020). Further, we assumed that there are no underlying temporal trends in abundance aside from those predicted by changes in environment. Given the low variability in oceanic conditions in our study area (Mann & Lazier, 2006) and long lifespans of false killer whales (Zaeschmar & Baird, 2026), we do not expect shifts in habitat preferences to play a significant role during the study period.

Variation in population size is certainly a possibility, given the population's documented interactions with fisheries, and may be accounted for in DSMs by including a year term in the encounter rate and/or group size model. However, sufficient sample sizes are required to ensure that the year term does not simply track the highly variable encounter rates over the survey period or serve as a proxy for unmeasured habitat variables (Becker et al. 2020). The sample size available for pelagic false killer whales in the central Pacific, especially when stratified by year, is insufficient to overcome these potential issues. Annual variation in abundance and sampling variability are confounded until we collect or integrate additional false killer whale data to allow accounting for temporal trends in population size. In the meantime, these models do account for shifts in distribution and abundance due to habitat variability and provide stable abundance estimates that are not strongly influenced by sampling variability.

The perpetual challenge of low sample sizes for cetaceans in the central Pacific may be mitigated by incorporating multiple data streams into future advancements of the DSM modeling framework. The most promising additional data type comes from a large effort to monitor the Pacific Islands region using passive acoustics, including hydrophone arrays towed behind the ship during visual surveys, seafloor-mounted hydrophones, drifting recorder buoys, and underwater gliders. These acoustic survey efforts have

yielded detection sample sizes that are orders of magnitude greater than visual surveys, particularly for cryptic species (e.g., Yano et al., 2025). DSMs integrating acoustic data are an area of active development (Sigourney et al., 2023) and are underway for pelagic false killer whales in the central Pacific.

Future research surveys should also be planned in areas of predicted high false killer whale density south of the Hawaiian EEZ to gather additional data to improve these models. PIFSC recently conducted the Survey for Continued Observation of Pseudorca Extent (SCOPE) beyond the southeastern extent of the Hawai‘i pelagic false killer whale assessment area, primarily aimed at collecting population-identifying data on false killer whale groups (e.g., genetic sampling, photo-identification, and satellite tag deployments). While SCOPE did not result in on-effort sightings of false killer whales, the acoustic data may be incorporated in future DSM efforts.

Conclusion

The model-based approach outlined here allowed for the estimation of pelagic false killer whale abundance at a variety of spatial scales within Hawaiian waters and the broader central Pacific. Our work updating this DSM framework provides a better characterization of the uncertainty in spatially-explicit false killer whale density estimates over the spatiotemporal range of interest, which is particularly important for efforts to assess and manage the Hawai‘i pelagic false killer whale population and mitigate impacts from interactions with longline fisheries. Additional sighting data, as well as integration of other data types, could allow us to account for population trends within the DSM framework and support robust management of this strategic stock. Further, this work has generated a reproducible workflow that can be applied to other cetacean species, increasing the efficiency and transparency of assessments in the Pacific Islands region and beyond.

Literature Cited

Ahrens, R. N. M., Bradford, A. L., Oleson, E. M., Crigler, E., & Fujita, K. (2025). Estimating non-U.S. longline fishing impacts on Hawai‘i pelagic false killer whales in a transboundary assessment area. *Conservation Science and Practice*, e70216.

Akaike, H. (1973). Information theory and an extension of the maximum likelihood principle. In B. N. Petrov and F. Csáki (Eds.), *2nd international symposium on information theory* (pp. 267–281). Budapest, Hungary: Akadémia Kiadó.

Allouche, O., Tsoar, A. & Kadmon, R. (2006). Assessing the accuracy of species distribution models: prevalence, kappa and the true skill statistic (TSS). *Journal of Applied Ecology, 43*, 1223–1232.

Alston, J. M., Fleming, C.H., Kays, R., Streicher, J. P., Downs, C. T., Ramesh, T., Reineking, B. & Calabrese, J. M. (2023). Mitigating pseudoreplication and bias in resource selection functions with autocorrelation-informed weighting. *Methods in Ecology and Evolution*, *14*, 643–654.

Anderson, P. A., Poe, R. B., Thompson, L. A., Weber, N., & Romano, T. A. (2017) Behavioral responses of beluga whales (*Delphinapterus leucas*) to environmental variation in an Arctic estuary. *Behavioural Processes, 145*, 48–59.

Baird, R. W., Gorgone, A. M., McSweeney, D. J., Webster, D. L., Salden, D. R., Deakos, M. H., Ligon, A. D., Schorr, G. S., Barlow, J., & Mahaffy, S. D. (2008). False killer whales (*Pseudorca crassidens*) around the main Hawaiian Islands: long-term site fidelity, inter-island movements, and association patterns. *Marine Mammal Science, 24*, 591–612.

Baird, R. W., Hanson, M. B., Schorr, G. S., Webster, D. L., McSweeney, D. J., Gorgone, A. M., Mahaffy, S. D., Holzer, D., Oleson, E. M., & Andrews, R. D. (2012). Assessment of range and primary habitats of Hawaiian insular false killer whales: informing determination of critical habitat. *Endangered Species Research, 18*, 47–61.

Baird, R. W., Oleson, E. M., Barlow, J., Ligon, A. D., Gorgone, A. M., & Mahaffy, S. D. (2013). Evidence of an island-associated population of false killer whales (*Pseudorca crassidens*) in the Northwestern Hawaiian Islands. *Pacific Science, 67*(4), 513–521.

Baird, R. W., Schorr, G. S., Webster, D. L., McSweeney, D. J., Hanson, M. B., & Andrews, R. D. (2010). Movements and habitat use of satellite-tagged false killer whales around the main Hawaiian Islands. *Endangered Species Research, 10*, 107–121.

Barlow, J. (2006). Cetacean abundance in Hawaiian waters estimated from a summer/fall survey in 2002. *Marine Mammal Science, 22*(2), 446–464.

Barlow, J. (2015). Inferring trackline detection probabilities, *g*(0), for cetaceans from apparent densities in different survey conditions. *Marine Mammal Science, 31*, 923–943.

Bayless, A. R., Oleson, E. M., Baumann-Pickering, S., Simonis, A. E., Marchetti, J., Martin, S., & Wiggins, S. M. (2017). Acoustically monitoring the Hawai‘i longline fishery for interactions with false killer whales. *Fisheries Research, 190*, 122–131.

Becker, E. A., Forney, K. A., Ferguson, M. C., Foley, D. G., Smith, R. C., Barlow, J., & Redfern, J. V. (2010). Comparing California Current cetacean-habitat models developed using in situ and remotely sensed sea surface temperature data. *Marine Ecology Progress Series*, *413*, 163–183.

Becker, E. A., Forney, K. A., Foley, D. G., & Barlow, J. (2012). *Density and spatial distribution patterns of cetaceans in the central North Pacific based on habitat models* (SWFSC Technical Memorandum Series, NOAA-TM-NMFS-SWFSC-490). Southwest Fisheries Science Center.

Becker, E. A., Forney, K. A., Fiedler, P. C., Barlow, J., Chivers, S. J., Edwards, C. A., Moore, A. M. & Redfern, J. V. (2016). Moving towards dynamic ocean management: How well do modeled ocean products predict species distributions? *Remote Sensing*, *8*(2),149.

Becker, E. A., Forney, K. A., Miller, D. L., Fiedler, P. C., Barlow, J., & Moore, J. E. (2020). *Habitat-based density estimates for cetaceans in the California Current Ecosystem based on 1991-2018 survey data* (SWFSC Technical Memorandum Series, NMFS-SWFSC-638). Southwest Fisheries Science Center.

Becker, E. A., Forney, K. A., Oleson, E. M., Bradford, A. L., Hoopes, R., Moore, J. E., & Barlow, J. (2022). *Abundance, distribution, and seasonality of cetaceans within the U.S. Exclusive Economic Zone around the Hawaiian Archipelago based on species distribution models* (PIFSC Technical Memorandum Series, NOAA-TM-NMFS-PIFSC-131). Pacific Islands Fisheries Science Center.

Becker, E. A., Forney, K. A., Thayre, B. J., Whitaker, K., Hoopes, R., Jones, J. M., Hildebrand, J. A., & Moore, J. (2025). Evaluating seasonal vs. spatial extrapolation for cetacean distribution models in the California Current. *Marine Mammal Science, 41*(4), e70030.

Bouchet, P., Miller, D. L., Roberts, J., Mannocci, L., Harris, C. M., & Thomas, L. (2019). From here and now to there and then: practical recommendations for extrapolating cetacean density surface models to novel conditions. Ref. CREEM Technical Report, no. 2019-1, University of St Andrews, St. Andrews, Scotland, UK.

Bouchet, P. J., Miller, D. L., Roberts, J. J., Mannocci, L., Harris, C. M. & Thomas, L. (2020). dsmextra: Extrapolation assessment tools for density surface models. *Methods in Ecology and Evolution*, *11*,1464–1469.

Bradford, A. L., Forney, K. A.,Oleson, E. M., & Barlow, J. (2014). Accounting for subgroup structure in line-transect abundance estimates of false killer whales (*Pseudorca crassidens*) in Hawaiian waters. *PLoS ONE*, *9*(2), e90464.

Bradford, A. L., Forney, K. A., Oleson, E. M., & Barlow, J. 2017. Abundance estimates of cetaceans from a line-transect survey within the U.S. Hawaiian Islands Exclusive Economic Zone. *Fishery Bulletin, 115*, 129–142.

Bradford, A. L., Oleson, E. M., Baird, R. W., Boggs, C. H., Forney, K. A., & Young, N. C. (2015). *Revised stock boundaries for false killer whales (Pseudorca crassidens) in Hawaiian waters* (PIFSC Technical Memorandum Series, NOAA-TM-NMFS-PIFSC-47). Pacific Islands Fisheries Science Center.

Bradford, A. L., Becker, E. A., Oleson, E. M., Forney, K. A., Moore, J. E., & Barlow, J. (2020). *Abundance estimates of false killer whales in Hawaiian waters and the broader central Pacific* (PIFSC Technical Memorandum Series, NOAA-TM-NMFS-PIFSC-104). Pacific Islands Fisheries Science Center.

Bravington, M. V., Miller, D. L. & Hedley, S. L. (2021). Variance propagation for density surface models. *Journal of Agricultural, Biological and Environmental Statistics*, *26*, 306–323.

Brooks, M. E., Kristensen, K., van Benthem, K. J., Magnusson, A., Berg, C. W., Nielsen, A., Skaug, H. J., Maechler, M., & Bolker, B. M. (2017). glmmTMB balances speed and

flexibility among packages for zero-inflated generalized linear mixed modeling. *The R Journal, 9*(2), 378–400.

Buckland, S. T., Anderson, D.R., Burnham, K. P., Laake, J. L., Borchers, D. L., & Thomas, L. (2001). Introduction to distance sampling. Estimating abundance of biological populations. Oxford, UK: Oxford University Press.

Carretta, J. V., Forney, K. A., Lowry, M. S., Barlow, J., Baker, J., Johnston, D., Hanson, B., Muto, M. M., Lynch, D., & Carswell, L. (2009). *U.S. Pacific marine mammal stock assessments: 2008* (NOAA Technical Memorandum NOAA-TM-NMFS-SWFSC-434). U.S. Dept. of Commerce.

Chelton, D. B., Schlax, M. G., & Samelson, R. M. (2011). Global observations of nonlinear mesoscale eddies. *Progress in Oceanography*, *91*(2),167-216.

Conn, P. B., Johnson, D. S., Williams, P. J., Melin, S. R., & Hooten, M. B. (2018). A guide to Bayesian model checking for ecologists. *Ecological Monographs*, *88*, 526-542.

Fader, J. E., Baird, R. W., Bradford, A. L., Dunn, D. C., Forney, K. A., & Read, A. J. (2021). Patterns of depredation in the Hawai‘i deep-set longline fishery informed by fishery and false killer whale behavior. *Ecosphere, 12*, e03682.

Fawcett, T. (2006). An introduction to ROC analysis. *Pattern Recognition Letters*, *27*, 861–874.

Ferguson, M. C., & Barlow, J. (2003). *Addendum: Spatial distribution and density of cetaceans in the eastern tropical Pacific Ocean based on summer/fall research vessel surveys in 1986–96* (SWFSC Administrative Report Series, LJ-01-04 (Addendum)). Southwest Fisheries Science Center.

Forney, K. A., Becker, E. A., Foley, D. G., Barlow, J., & Oleson, E. M. (2015). Habitat-based models of cetacean density and distribution in the central North Pacific. *Endangered Species Research, 27*(1), 1–20.

Forney, K. A., Kobayashi, D. R., Johnston, D. W., Marchetti, J. A., & Marsik, M. G. (2011). What’s the catch? Patterns of cetacean bycatch and depredation in Hawaii-based pelagic longline fisheries. *Marine Ecology*, *32*(3), 380–391

Geng, X., Kug, J. S., Shin, N. Y., Zhang, W, & Chen, H. C. (2024). On the spatial double peak of the 2023-2024 El Niño event. *Communications Earth & Environment*, *5*, 691.

Gerrodette, T., & Forcada, J. (2005). Non-recovery of two spotted and spinner dolphin populations in the eastern tropical Pacific Ocean. *Marine Ecology Progress Series 291*, 1-21.

Givens, G. H., & Hoeting, J. A. (2012). *Computational statistics*. John Wiley & Sons.

Guevara, L, Gerstner, B. E., Kass, J. M., & Anderson, R. P. (2018). Toward ecologically realistic predictions of species distributions: A cross-time example from tropical montane cloud forests. *Global Change Biology, 24*(4), 1511-1522.

Hamilton, T. A., Redfern, J. V., Barlow, J., Ballance, L. T., Gerrodette, T., Holt, R. S., Forney, K. A., & Taylor, B. L. (2009). *Atlas of cetacean sightings for Southwest Fisheries Science Center cetacean and ecosystem surveys, 1986–2005* (SWFSC Technical Memorandum Series, NMFS-SWFSC-440). Southwest Fisheries Science Center.

Hanks, E. M., & Hughes, D. A. (2016). Flexible discrete space models of animal movement. *arXiv:1606.07986*.

Hedley, S. L., & Buckland, S. T. (2004). Spatial models for line transect sampling. *Journal of Agricultural, Biological, and Environmental Statistics*, *9*(2), 181–199.

Hijmans, R. (2025). *terra: Spatial Data Analysis*. R package version 1.8–81. https://github.com/rspatial/terra.

Hu, F., & Zidek, J. V. (2002). The weighted likelihood. *Canadian Journal of Statistics*, *30*(3), 347–371.

Kinzey D., Olson P., & Gerrodette T. (2000). *Marine mammal data collection procedures on research ship line-transect surveys by the Southwest Fisheries Science Center* (SWFSC Administrative Report Series, LJ-00-08). Southwest Fisheries Science Center.

Liu, C., Berry, P. M., Dawson, T. P. & Pearson, R. G. (2005). Selecting thresholds of occurrence in the prediction of species distributions. *Ecography*, *28*, 385–393.

Lunardon, N., Menardi, G. & Torelli, N. (2014). ROSE: a package for binary imbalanced learning. *The R Journal*, *6*, 79–89.

Mann, K. H., & Lazier, J. R. N. (2006). Dynamics of Marine Ecosystems: Biological-Physical Interactions in the Oceans (3rd ed.). Malden, MA: Blackwell Publishing.

Mannocci, L., Monestiez, P., Spitz, J., & Ridoux, V. (2015). Extrapolating cetacean densities beyond surveyed regions: habitat-based predictions in the circumtropical belt. *Journal of Biogeography*, *42*(7), 1267–1280.

Mannocci, L., Roberts, J. J., Pedersen, E. J. & Halpin, P. N. (2020). Geographical differences in habitat relationships of cetaceans across an ocean basin. *Ecography*, *43*, 1250-1259.

Marra, G., & Wood, S. N. (2011). Practical variable selection for generalized additive models. *Computational Statistics and Data Analysis*, *55*(7), 2372–2387.

Marra, G. & Wood, S. N. (2012). Coverage properties of confidence intervals for generalized additive model components. *Scandinavian Journal of Statistics*, *39*, 53–74.

Martien, K. K., Chivers, S. J., Baird, R. W., Archer, E., Gorgonne, A. M., Hancock, B. L., Matilla, D., McSweeney, D. J., Oleson, E. M., Palmer, C. L., Pease, V., Robertson, K. M., Robbins, J., Schorr, G. S., Schultz, M., Webster, D. L., & Taylor B. L. (2014). Nuclear and mitochondrial patterns of population structure in North Pacific false killer whales (*Pseudorca crassidens*). *Journal of Heredity*, *105*(5), 611–626.

Menardi, G., & Torelli, N. (2014). Training and assessing classification rules with imbalanced data. *Data Mining and Knowledge Discovery*, *28*, 92–122.

Miller, D. L., Burt, M. L., Rexstad, E. A., & Thomas, L. (2013). Spatial models for distance sampling data: recent developments and future directions. *Methods in Ecology and Evolution*, *4*(11), 1001–1010.

Miller, D. L., Rexstad, E., Thomas, L., Marshall, L., & Laake, J. L. (2019). Distance sampling in R. *Journal of Statistical Software*, *89*(1), 1–28.

Miller, D. L., Becker, E. A., Forney, K. A., Roberts, J. J., Cañadas, A., & Schick, R. S., (2022). Estimating uncertainty in density surface models. *PeerJ*, *10*, e13950.

Miller, D. L. (2025). *dsm: Density Surface Modelling of Distance Sampling Data*. R package version 2.3.4. https://github.com/DistanceDevelopment/dsm

NMFS. (2023). *Guidelines for Preparing Stock Assessment Reports Pursuant to the Marine Mammal Protection Act*. Protected Resources Policy Directive Marine Mammal Protection Act. 02-204.

Oleson, E. M., Boggs, C. H., Forney, K. A., Hanson, M. B., Kobayashi, D. R., Taylor, B. L., Wade, P. R., & Ylitalo, G. M. (2010). *Status review of Hawaiian insular false killer whales (*Pseudorca crassidens*) under the Endangered Species Act* (PIFSC Technical

Memorandum Series, NOAA-TM-NMFS-PIFSC-22). Pacific Islands Fisheries Science Center.

Oleson, E. M., Bradford, A. L., & Martien, K. M. (2023). *Developing a management area for Hawai'i pelagic false killer whales* (PIFSC Technical Memorandum Series, NMFS-PIFSC-150, 2525). Pacific Islands Fisheries Science Center.

Pya, N., & Wood, S. N. (2015). Shape constrained additive models. *Statistical Computing, 25*, 543–559.

Rankin, S., Oedekoven, C., & Archer, F. (2020). Mark recapture distance sampling: using acoustics to estimate the fraction of dolphins missed by observers during shipboard line-transect surveys. *Environmental and Ecological Statistics 27*, 233–251.

Redfern, J. V., Moore, T. J., Fiedler, P. C., de Vos, A., Brownell, R. L., Forney, K. A., Becker, E. A., & Ballance, L. T. (2017). Predicting cetacean distributions in data-poor marine ecosystems. *Diversity & Distributions*, *23*(4), 394–408.

Roberts, J. J., Best, B. D., Mannocci, L., Fujioka, E., Halpin, P. N., Palka, D. L., Garrison, L. P., Mullin, K. D., Cole, T. V., Khan, C. B., McLellan, W. A., Pabst, D. A., & Lockhart, G. G. (2016). Habitat-based cetacean density models for the U.S. Atlantic and Gulf of Mexico. *Scientific Reports*, *6*, 22615.

Sigourney, D. B., DeAngelis, A., Cholewiak, D., & Palka, D. (2023). Combining passive acoustic data from a towed hydrophone array with visual line transect data to estimate abundance and availability bias of sperm whales (*Physeter macrocephalus*). *PeerJ*, *11*, e15850.

Thomas, L., Williams, R., & Sandilands, D. (2007). Designing line transect surveys for complex regions. *Journal of Cetacean Research and Management*, *9*(1), 1–13.

Wang, S. X. (2001). Maximum weighted likelihood estimation. PhD diss., University of British Columbia.

Wood, S. N. (2011). Fast stable restricted maximum likelihood and marginal likelihood estimation of semiparametric generalized linear models. *Journal of the Royal Statistical Society B*, *73*, 3–36.

Wood, S. N. (2017). Generalized additive models: An introduction with R, 2nd edition. New York, USA: CRC Press.

Woodman, S. (2025). swfscDAS: Processing DAS Data Files. R package version 0.6.4, https://swfsc.github.io/swfscDAS/.

Yano, K. M., Oleson, E. M., Keating, J. L., Ballance, L. T., Hill, M. C., Bradford, A. L., Allen, A. N., Joyce, T. W., Moore, J. E., & Henry, A. E. (2018). *Cetacean and seabird data collected during the Hawaiian Islands Cetacean and Ecosystem Assessment Survey (HICEAS), July–December 2017* (PIFSC Technical Memorandum Series, NMFS-PIFSC-72). Pacific Islands Fisheries Science Center.

Yano, K. M., Oleson, E. M., McCullough, J. L. K., Hill, M, C., & Henry, A. E. (2020). *Cetacean and seabird data collected during the Winter Hawaiian Islands Cetacean and Ecosystem Assessment Survey (Winter HICEAS), January–March 2020* (PIFSC Technical Memorandum Series, NOAA-TM-NMFS-PIFSC-111). Pacific Islands Fisheries Science Center.

Yano, K. M., Oleson, E. M., McCullough J. L. K., Hill, M. C., Bradford, A. L., Joyce, T. W., Suca, J. J., Whitney, J. L., & Henry, A. E. (2025). *Cetacean and seabird data collected during*

the Hawaiian Islands Cetacean and Ecosystem Assessment Survey (HICEAS), July–December 2023 (PIFSC Technical Memorandum. NMFS-PIFSC-175). Pacific Islands Fisheries Science Center.

Zaeschmar, J., & Baird, R. W. (2026). False killer whale *Pseudorca crassidens* (Owen, 1846). In Oceanic Dolphins (pp. 537-587). Academic Press.

Tables

Table 1. Summary of ship-based line-transect surveys conducted by Southwest Fisheries Science Center and Pacific Islands Fisheries Science Center in the central and eastern Pacific between 1986 and 2023 that encountered false killer whales (*n* = 40). Effort and qualifying sightings made during surveys inside the central Pacific study area (Figure 1) were used in the density surface model (DSM), and effort and sightings outside the study area were used to supplement the detection parameter estimation.

Year	Survey	On-effort Survey Distance (km)	Survey Period	Focal Region	Analysis Contribution
1986	0989	16,528	Jul–Dec	Eastern tropical Pacific	Detection parameters
1986	0990	14,021	Aug–Dec	Eastern tropical Pacific	Detection parameters
1987	1080	16,135	Jul–Dec	Eastern tropical Pacific	Detection parameters
1987	1081	13,942	Aug–Dec	Eastern tropical Pacific	Detection parameters
1988	1164	11,979	Jul–Dec	Eastern tropical Pacific	Detection parameters
1988	1165	13,568	Jul–Dec	Eastern tropical Pacific	Detection parameters
1989	1268	14,976	Jul–Dec	Eastern tropical Pacific	Detection parameters
1990	1369	13,999	Aug–Dec	Eastern tropical Pacific	Detection parameters
1990	1370	19,042	Jul–Dec	Eastern tropical Pacific	Detection parameters
1992	1467	10,676	Aug–Nov	Eastern tropical Pacific	Detection parameters
1993	1509	11,208	Jul–Nov	California, Eastern tropical Pacific	Detection parameters
1997	1607	7,480	Mar–Jun	Temperate North Pacific	DSM and detection parameters
1998	1610	15,397	Jul–Dec	Eastern tropical Pacific	Detection parameters
1998	1611	16,631	Jul–Dec	Eastern tropical Pacific	DSM and detection parameters
1998	1612	12,351	Jul–Dec	Eastern tropical Pacific	Detection parameters
1999	1613	13,740	Jul–Dec	Eastern tropical Pacific	Detection parameters
1999	1614	16,975	Jul–Dec	Eastern tropical Pacific	DSM and detection parameters
2000	1615	13,835	Jul–Dec	Eastern tropical Pacific	Detection parameters
2000	1616	17,443	Jul–Dec	Eastern tropical Pacific	Detection parameters
2002	1621	16,947	Jul–Dec	Hawaiian EEZ	DSM and detection parameters
2002	1622	7,678	Oct–Dec	Hawaiian EEZ	DSM and detection parameters
2003	1623	14,359	Jul–Dec	Eastern tropical Pacific	Detection parameters
2003	1624	11,989	Jul–Dec	Eastern tropical Pacific	Detection parameters
2005	1629	15,714	Jul–Nov	Central Pacific islands	DSM and detection parameters
2006	1630	8,965	Jul–Dec	Eastern tropical Pacific	Detection parameters
2006	1631	14,830	Jul–Dec	Eastern tropical Pacific	DSM and detection parameters
2007	1634	9,578	Aug–Nov	Eastern tropical Pacific	Detection parameters

Year	Survey	On-effort Survey Distance (km)	Survey Period	Focal Region	Analysis Contribution
2009	0901	2,361	Feb	Main Hawaiian Islands	DSM and detection parameters
2010	1004	1,131	Apr–May	Central Pacific transit	DSM and detection parameters
2010	1641	16,305	Aug–Dec	Hawaiian EEZ	DSM and detection parameters
2010	1642	7,486	Sep–Oct	Hawaiian EEZ	DSM and detection parameters
2011	1108	4,022	Oct–Nov	Palmyra Atoll	DSM and detection parameters
2012	1203	2,998	Apr–May	Palmyra Atoll	DSM and detection parameters
2013	1303	4,274	May–Jun	Northwestern Hawaiian Islands	DSM and detection parameters
2016	1604	3,332	Jun–Jul	Main Hawaiian Islands	DSM and Detection parameters
2017	1705	12,120	Aug–Dec	Hawaiian EEZ	DSM and detection parameters
2017	1706	11,703	Jul–Oct	Hawaiian EEZ	DSM and detection parameters
2020	2001	5,268	Jan–Mar	Main Hawaiian Islands	DSM and detection parameters
2023	2303	15,015	Jul–Dec	Hawaiian EEZ	DSM and detection parameters
2023	2401	5,168	Oct–Dec	Hawaiian EEZ	DSM and detection parameters

Table 2. Details of pelagic false killer whale sightings (*n* = 44) made on line-transect surveys (*n* = 20) conducted by Southwest or Pacific Islands Fisheries Science Centers, 1997–2023, within the central Pacific study area. Effort types are systematic (S) or nonsystematic (N). See text for: 1) details of uncertain population assignment in areas of overlap with insular false killer whale populations in the main Hawaiian Islands (MHI) and Northwestern Hawaiian Islands (NWHI), and 2) explanations of the actual or expected number of subgroups and effective group size for each sighting.

Year	Survey	Ship-Sighting No.	Effort Type	Population	Number of Subgroups	Effective Group Size
1997	1607	MAC-200	S	Hawai‘i Pelagic	3.02	6.82
1998	1611	END-130	N	Unknown Pelagic	2.13	4.82
1999	1614	MAC-68	S	Unknown Pelagic	1.63	3.69
2002	1621	DSJ-184	S	Hawai‘i Pelagic	2.92	6.61
2005	1629	MII-151	S	Unknown Pelagic	1.89	4.28
2005	1629	MII-155	S	Unknown Pelagic	1.37	3.09
2005	1629	MII-200	S	Hawai‘i Pelagic	1.25	2.82
2005	1629	MII-204	S	Hawai‘i Pelagic	2.20	4.99
2005	1629	MII-207	S	Hawai‘i Pelagic	0.94	2.12
2005	1629	MII-216	S	Unknown Pelagic	1.85	4.18
2005	1629	MII-219	S	Unknown Pelagic	2.49	5.64
2006	1631	MII-120	S	Unknown Pelagic	1.32	2.99
2006	1631	MII-128	S	Unknown Pelagic	3.52	7.96
2009	901	OES-49	S	MHI or Hawai‘i Pelagic	0.94	2.12
2009	901	OES-79	S	MHI or Hawai‘i Pelagic	0.96	2.17
2010	1004	OES-5	S	Unknown Pelagic	2.52	5.69
2010	1641	MII-35	S	Hawai‘i Pelagic	3.20	7.23
2010	1641	MII-98	S	MHI or Hawai‘i Pelagic	1	2.26
2010	1641	MII-103	S	Hawai‘i Pelagic	1	2.26
2010	1641	MII-231	S	Hawai‘i Pelagic	1	2.26
2010	1641	MII-241	S	Hawai‘i Pelagic	6.44	14.55
2011	1108	OES-4	S	Unknown Pelagic	4	9.05
2012	1203	OES-69	N	Unknown Pelagic	1	2.26
2013	1303	OES-13	S	NWHI or Hawai‘i Pelagic	2	4.52

Year	Survey	Ship-Sighting No.	Effort Type	Population	Number of Subgroups	Effective Group Size
2013	1303	OES-59	S	Hawai‘i Pelagic	1.50	3.39
2013	1303	OES-62	S	NWHI or Hawai‘i Pelagic	4	9.05
2017	1705	LAS-55	N	MHI or Hawai‘i Pelagic	1	2.26
2017	1705	LAS-56	N	MHI or Hawai‘i Pelagic	3	6.78
2017	1705	LAS-64	S	Hawai‘i Pelagic	2	4.52
2017	1705	LAS-73	S	Hawai‘i Pelagic	6	13.57
2017	1705	LAS-125	N	NWHI or Hawai‘i Pelagic	6	13.57
2017	1705	LAS-159	N	Hawai‘i Pelagic	1	2.26
2017	1706	OES-1	N	MHI or Hawai‘i Pelagic	3	6.78
2017	1706	OES-33	S	Hawai‘i Pelagic	4	9.05
2017	1706	OES-39	S	Hawai‘i Pelagic	4	9.05
2017	1706	OES-119	N	Hawai‘i Pelagic	11	24.88
2017	1706	OES-122	S	Hawai‘i Pelagic	3	6.78
2017	1706	OES-133	S	NWHI or Hawai‘i Pelagic	6	13.57
2017	1706	OES-141	S	Hawai‘i Pelagic	1	2.26
2020	2001	OES-131	S	MHI or Hawai‘i Pelagic	7.44	16.83
2020	2001	OES-255	S	Hawai‘i Pelagic	1	2.26
2020	2001	OES-258	N	MHI or Hawai‘i Pelagic	4	9.05
2020	2001	OES-285	S	Hawai‘i Pelagic	2	4.52
2023	2303	OES-198	S	NWHI or Hawai‘i Pelagic	5	11.31

Table 3. Beaufort-specific estimates of trackline detection probability, *g*(0), and effective strip width, *ESW*, for false killer whales in Beaufort sea states (b) 0–6 along with corresponding number of sightings (*n*). The intervals in brackets are 95% confidence intervals for the estimated quantities.

Parameter	**b0**	**b1**	**b2**	**b3**	**b4**	**b5**	**b6**
n	4	6	15	34	44	25	7
***g*(0)**	1.0	1.0	0.70 [0.64–0.75]	0.49 [0.41–0.57]	0.34 [0.26–0.43]	0.23 [0.17–0.32]	0.16 [0.10–0.23]
***ESW* (km)**	3.87 [2.93–4.79]	3.55 [2.72–4.34]	3.22 [2.59–3.84]	2.88 [2.49–3.32]	2.56 [2.26–2.87]	2.25 [1.92–2.59]	1.98 [1.56–2.44]

Table 4. Resulting abundance estimates of pelagic false killer whales in 2024 in retrospective estimates leaving out each of the four large-scale Hawaiian Islands Cetacean Ecosystem and Assessment Surveys (HICEAS) at each fold. *nf* represents the resulting sample size after omitting data from the specified survey. The coefficient of variation (CV) is included to reflect variability in estimates across folds relative to the magnitude of estimates. Note: As variance propagation was not conducted on these estimates, the 95% confidence intervals (CIs) are not comparable to those reported in Table 5.

HICEAS Removed	n_f	**Central Pacific Abundance [95% CI]**	**Assessment Area Abundance [95% CI]**	**Hawaiian EEZ Abundance [95% CI]**
2002	43	35,199 [20,352–50,046]	5,704 [3,681–7,727]	2,213 [1,437–2989]
2010	38	37,033 [19,201–54,865]	4,816 [2,991–6,641]	1,844 [1,095–2,593]
2017	31	27,363 [21,885–32,841]	3,105 [2,382–3,828]	1,108 [879–1,337]
2023	43	30,614 [20,600–40,628]	5,928 [3,468–8,388]	2,465 [1,475–3,455]
CV		0.12	0.23	0.27

Table 5. Model-based abundance estimates of pelagic false killer whales in the central Pacific, the Hawai‘i pelagic false killer whale assessment area, and the U.S. Exclusive Economic Zone around the Hawaiian Islands (Hawaiian EEZ) during 2020–2024, with predictions for 2017 included as a point of comparison with previous estimates reported in Bradford et al. (2020).

Region	Abundance Estimate [95% CI]	CV
Central Pacific (25,177,036 km^2)		
Avg. 2020–2024	33,216 [9,917–82,950]	0.58
2017	32,471 [11,111–74,879]	0.52
2020	30,956 [10,494–71,778]	0.52
2021	29,081 [10,294–65,697]	0.50
2022	24,811 [9,006–55,192]	0.49
2023	45,598 [15,424–105,881]	0.52
2024	35,634 [12,044–82,784]	0.52
Assessment Area (6,763,991 km^2)		
Avg. 2020–2024	4,526 [1,547–10,444]	0.52
2017	4,647 [1,453–11,300]	0.56
2020	4,933 [1,676–11,423]	0.52
2021	4,124 [1,486–9,216]	0.49
2022	4,467 [1,485–10,482]	0.53
2023	4,262 [1,483–9,731]	0.51
2024	4,843 [1,715–10,939]	0.50
Hawaiian EEZ (2,497,041 km^2)		
Avg. 2020–2024	1,745 [526–4,334]	0.58
2017	1,828 [489–4,852]	0.64
2020	1,950 [580–4,882]	0.59
2021	1,545 [510–3,642]	0.54
2022	1,744 [483–4,541]	0.62
2023	1,639 [523–3,940]	0.55
2024	1,848 [602–4,390]	0.54

Figures

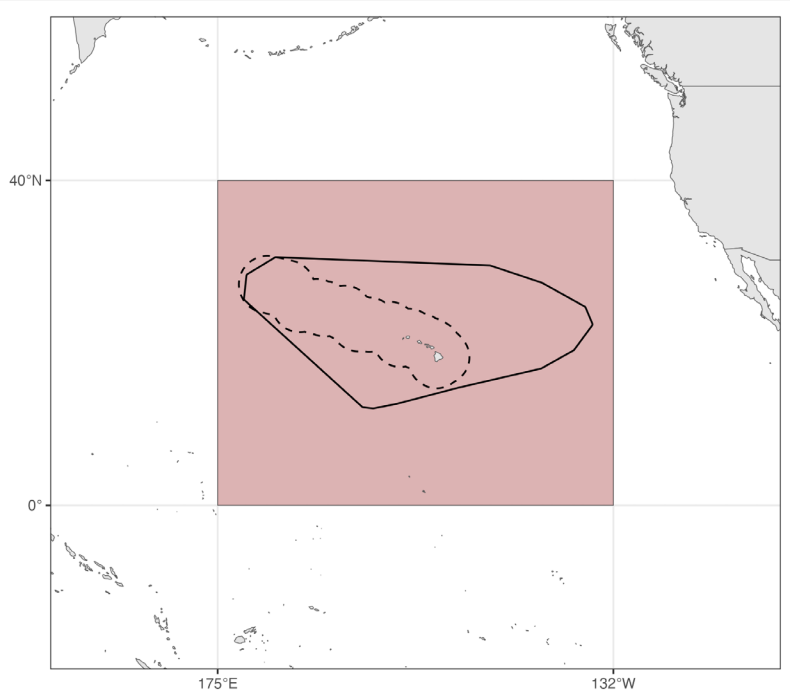

Figure 1. The central Pacific study area (rose shading) with enclosed Hawai‘i pelagic false killer whale assessment area (solid black line; Oleson et al. 2023) and the U.S. Exclusive Economic Zone around the Hawaiian Islands (dashed black line).

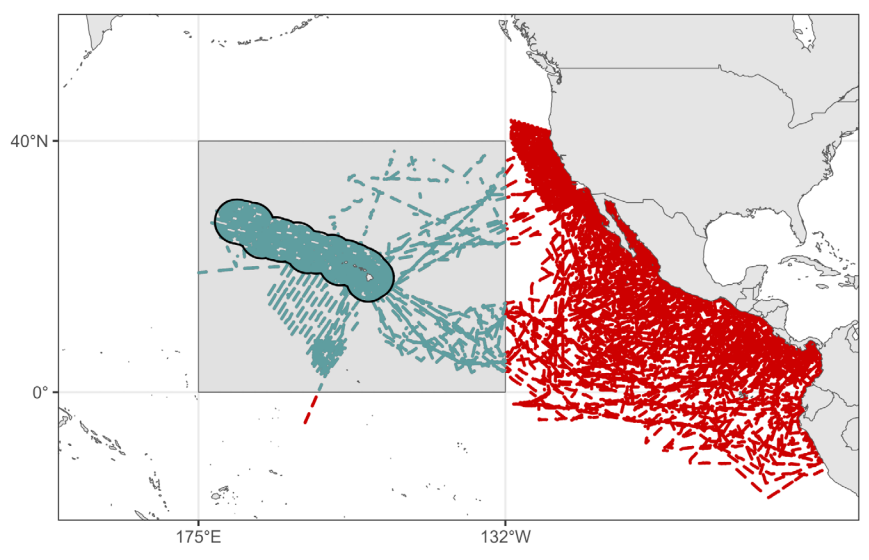

Figure 2. Ship-based survey tracklines for data used in the estimation framework (Table 1). Data (sightings and effort) from red tracklines were used for detection parameter estimation only; data from blue tracklines within the central Pacific study area (gray shading) were used for both detection parameter estimation and density estimation.

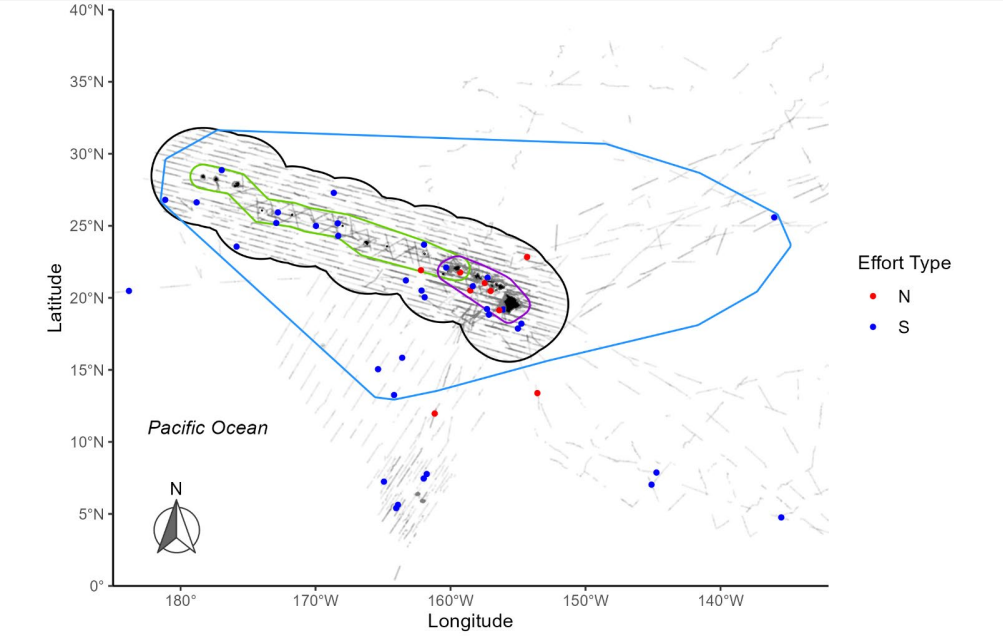

Figure 3. Locations of false killer whale sightings (*n* = 44) used for pelagic false killer whale density estimation made while on-effort during line-transect surveys in Beaufort 0–6 within the central Pacific study area. Red and blue dots are sightings made during non-systematic (*n* = 9) or systematic effort (*n* = 35), respectively, with associated tracklines in gray. Lines represent the U.S. Exclusive Economic Zone around the Hawaiian Islands (black), the Hawai‘i pelagic stock assessment area (blue), the insular main Hawaiian Islands stock boundary (purple) and the Northwestern Hawaiian Islands stock boundary (green).

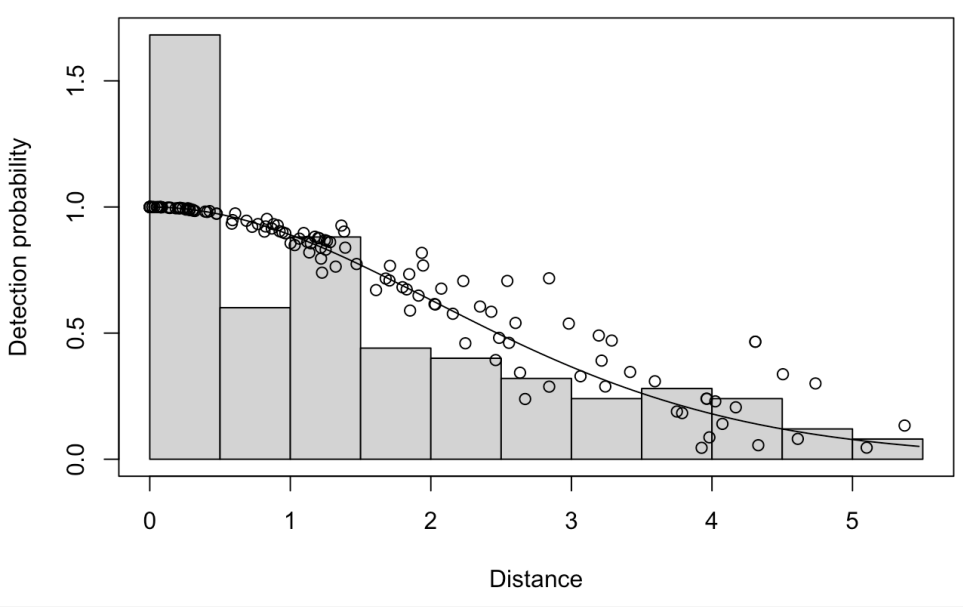

Figure 4. Histogram of systematic and nonsystematic false killer whale sightings (*n* = 135) by perpendicular distance from the trackline, along with the fitted half-normal model used to estimate the detection function.

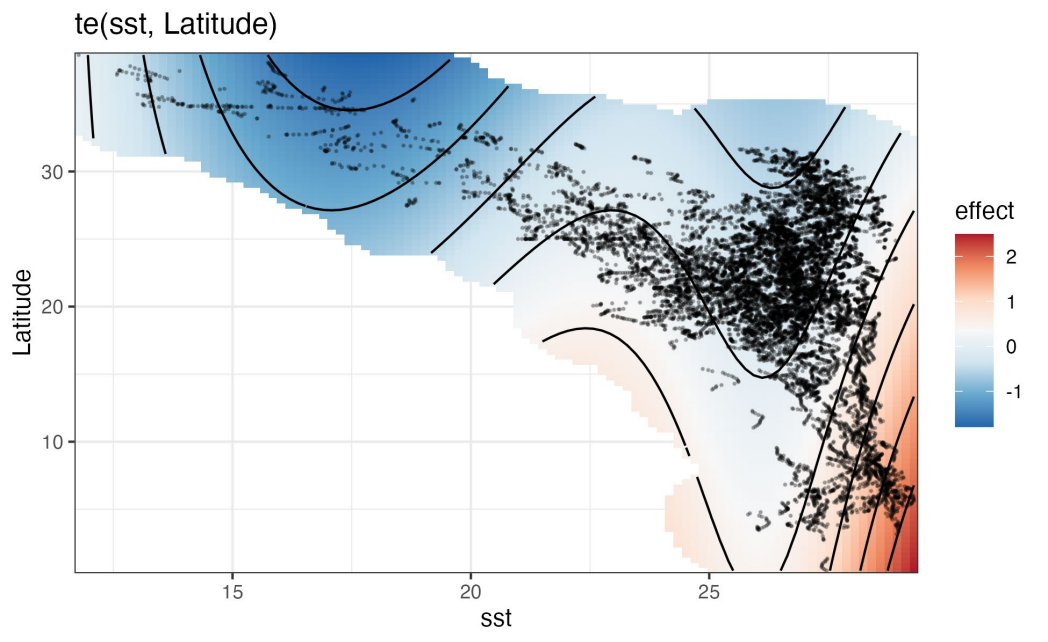

Figure 5. Estimated bivariate smooth effect of sea surface temperature (sst) and latitude (northern latitudes) in the final encounter rate model of pelagic false killer whales in the central Pacific study area. Contour values indicate the influence of the smooth (blue = low, red = high). Black dots are the covariate values observed at the survey segment days and locations.

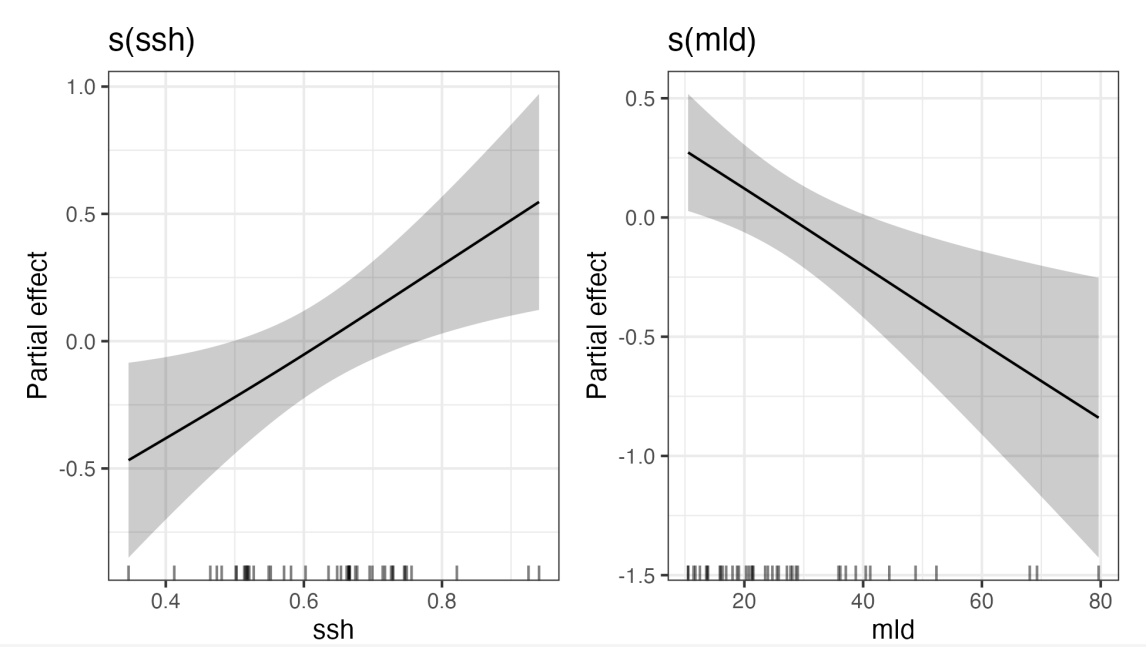

Figure 6. Estimated functional relationships between the habitat variables and group size in the final model of pelagic false killer whales in the central Pacific study area. Variables included sea surface height (ssh) and mixed layer depth (mld). The y-axes represent the term's partial effect, with shading indicating 2x standard error bands (i.e., 95% confidence interval); tick marks above the x-axes show data values.

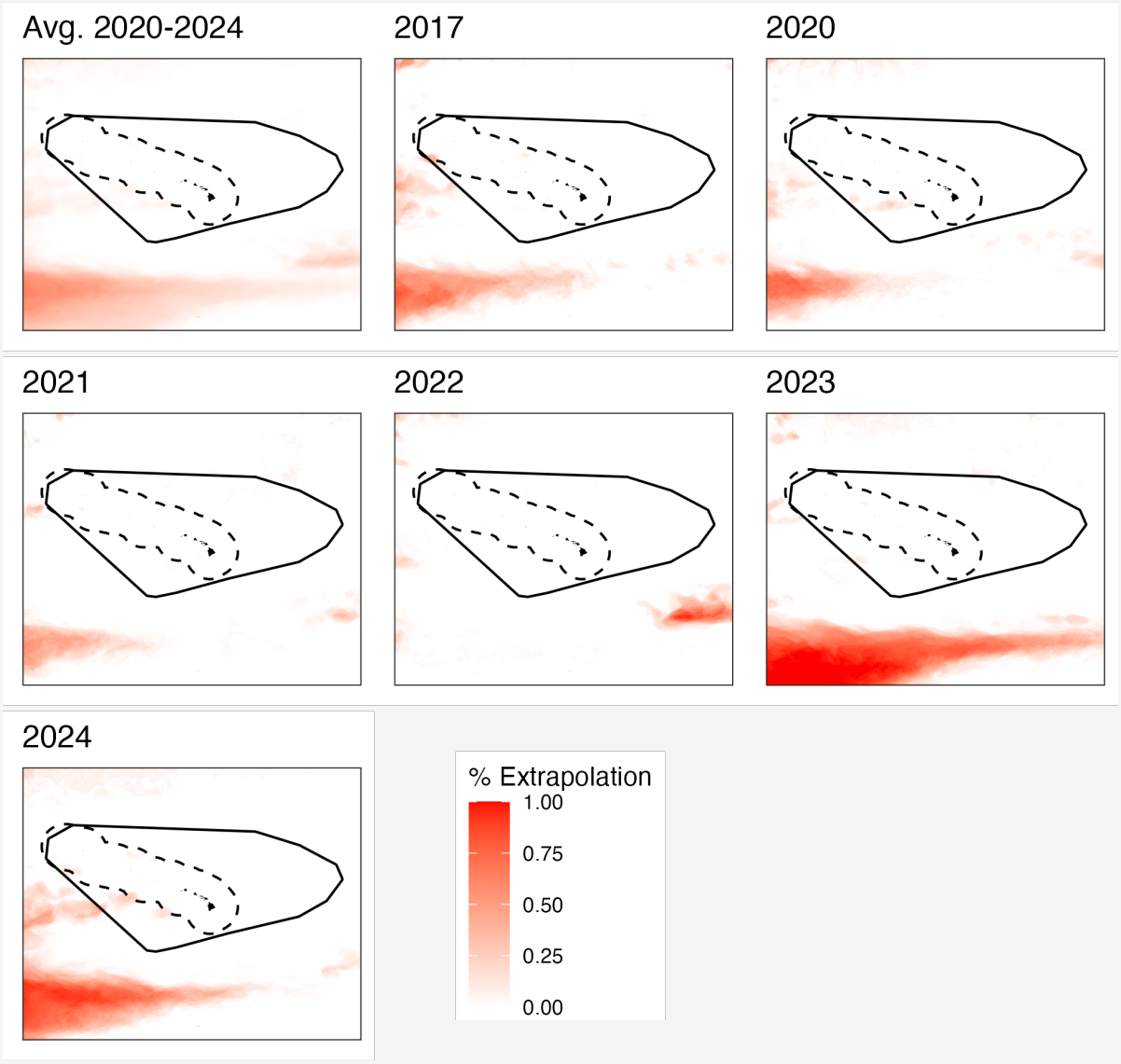

Figure 7. Visualization of extrapolation from the density surface model (DSM) dataset, which includes data mainly sampled within or close to the U.S. Exclusive Economic Zone around the Hawaiian Islands (dashed black line), in projecting the DSM output to the study area (figure extent). Method of diagnosing extrapolation conditions encompasses both univariate and combinatorial extrapolation. Solid black line represents the Hawai‘i pelagic false killer whale assessment area. Pixel color represents the proportion of prediction days that the environmental covariate values in each cell lie outside of sampled covariate value ranges (i.e., extrapolation conditions), where deeper red hues indicate more days in extrapolation conditions.

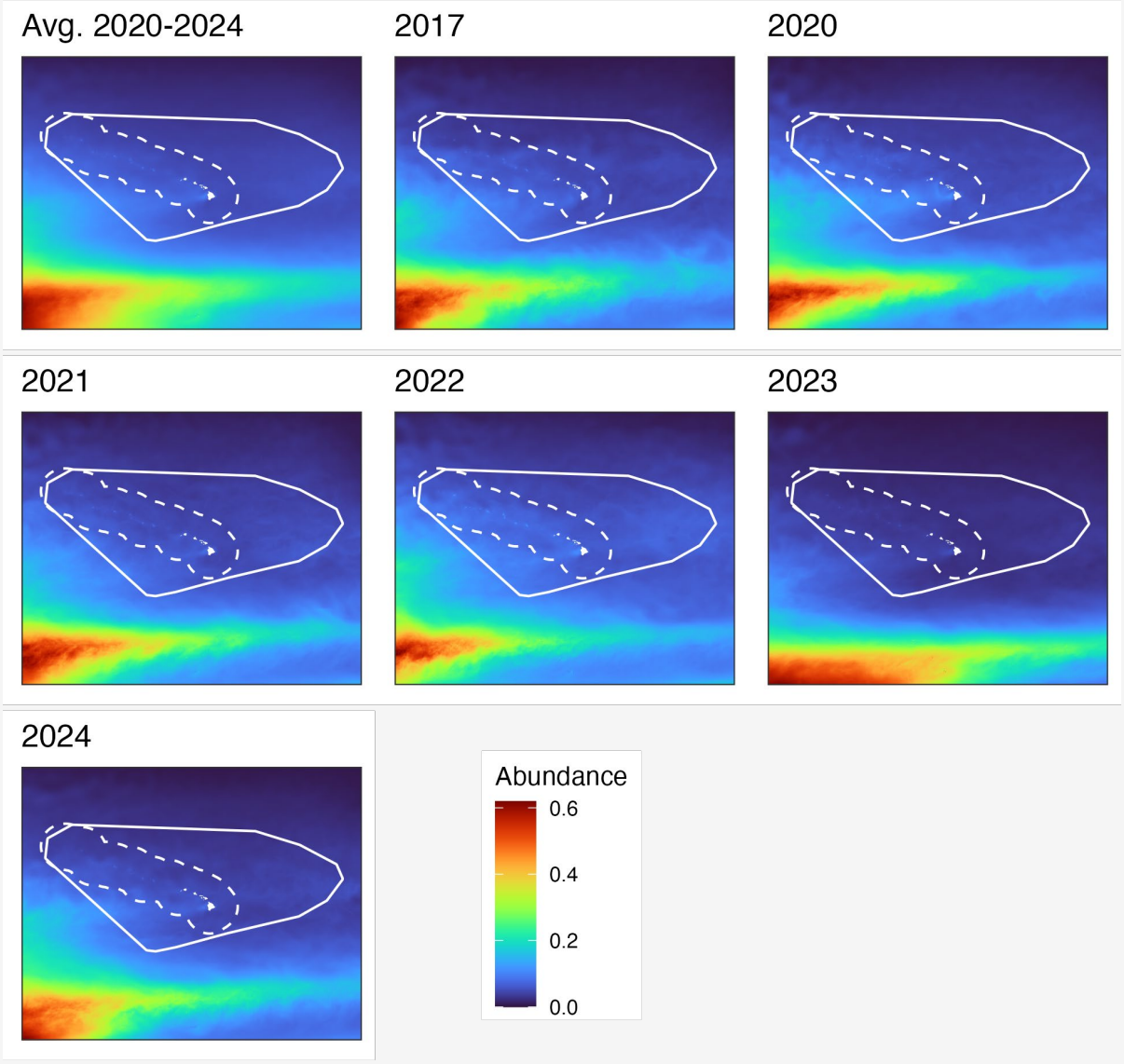

Figure 8. Yearly average spatial abundance predictions for pelagic false killer whales in the central Pacific study area. Lines represent the U.S. Exclusive Economic Zone around the Hawaiian Islands (dashed) and the Hawai‘i pelagic false killer whale assessment area (solid). Pixel color represents the expected number of individuals in each pixel.

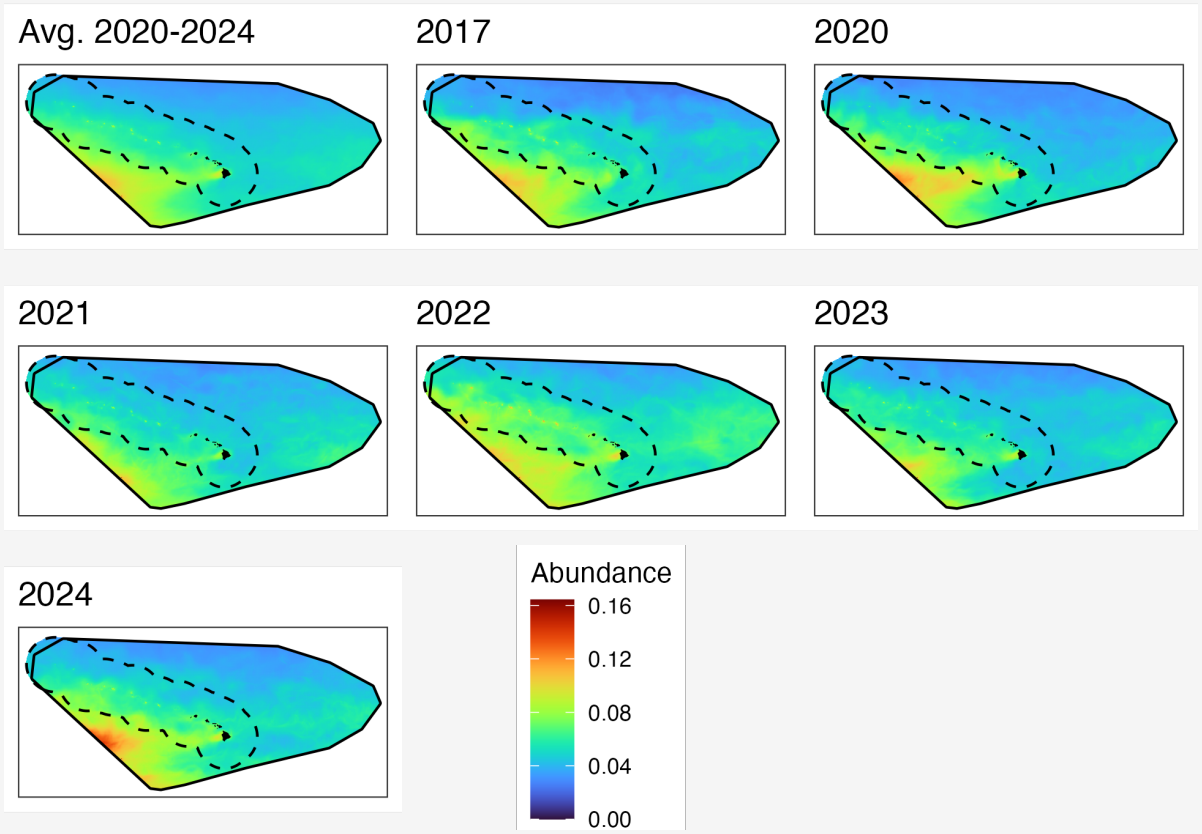

Figure 9. Yearly average spatial abundance predictions for pelagic false killer whales in the U.S. Exclusive Economic Zone around the Hawaiian Islands (dashed line) and the Hawai‘i pelagic false killer whale assessment area (solid line). Pixel color represents the expected number of individuals in each pixel.

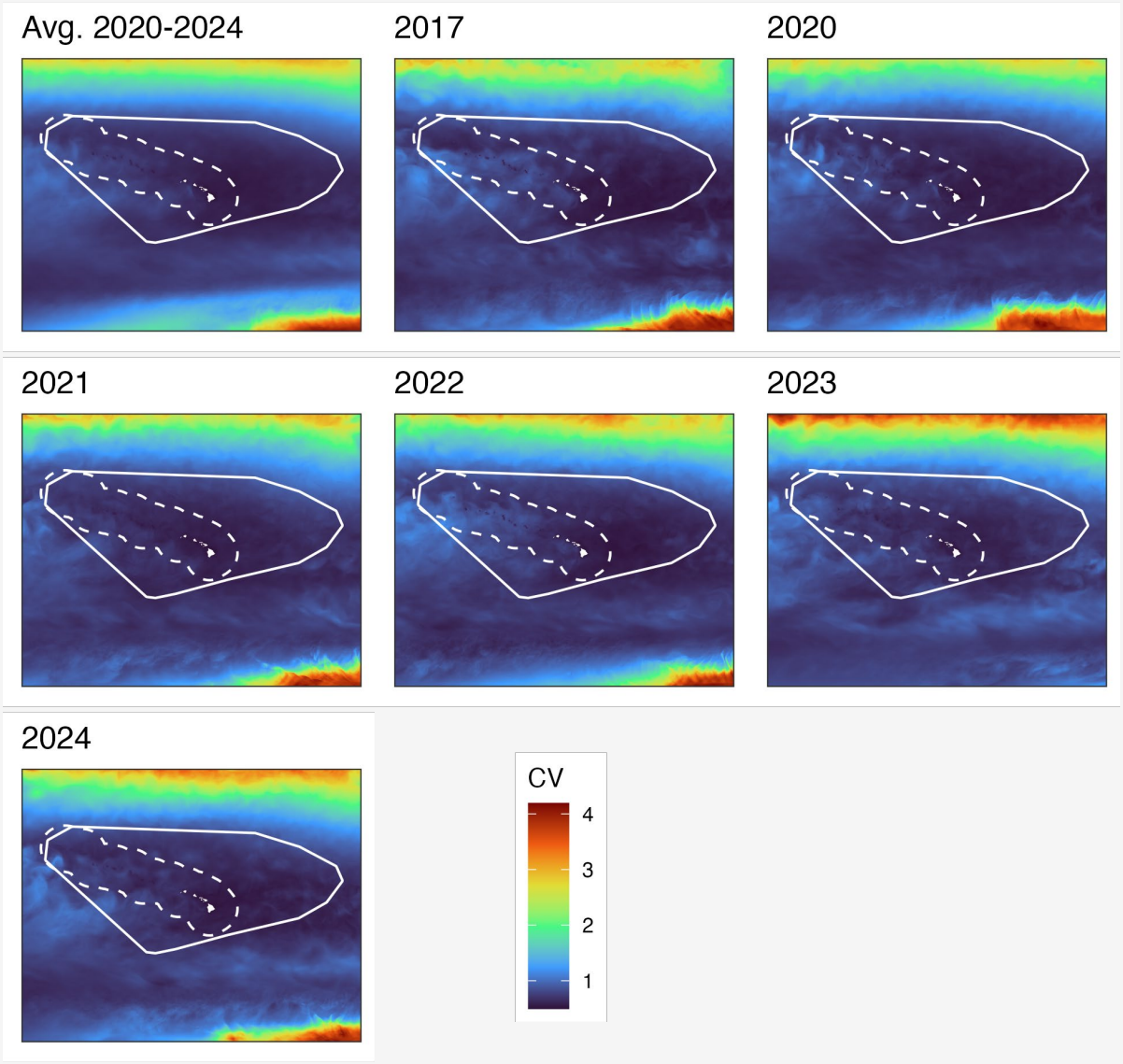

Figure 10. Spatially-explicit estimates of the abundance prediction coefficient of variation (CV) in pelagic false killer whale abundance in the central Pacific study area. Lines represent the U.S. Exclusive Economic Zone around the Hawaiian Islands (dashed) and Hawai‘i pelagic false killer whale assessment area (solid). Pixel color represents the CV in each pixel. Survey effort tracks are overlayed in this figure on the linked vignette.

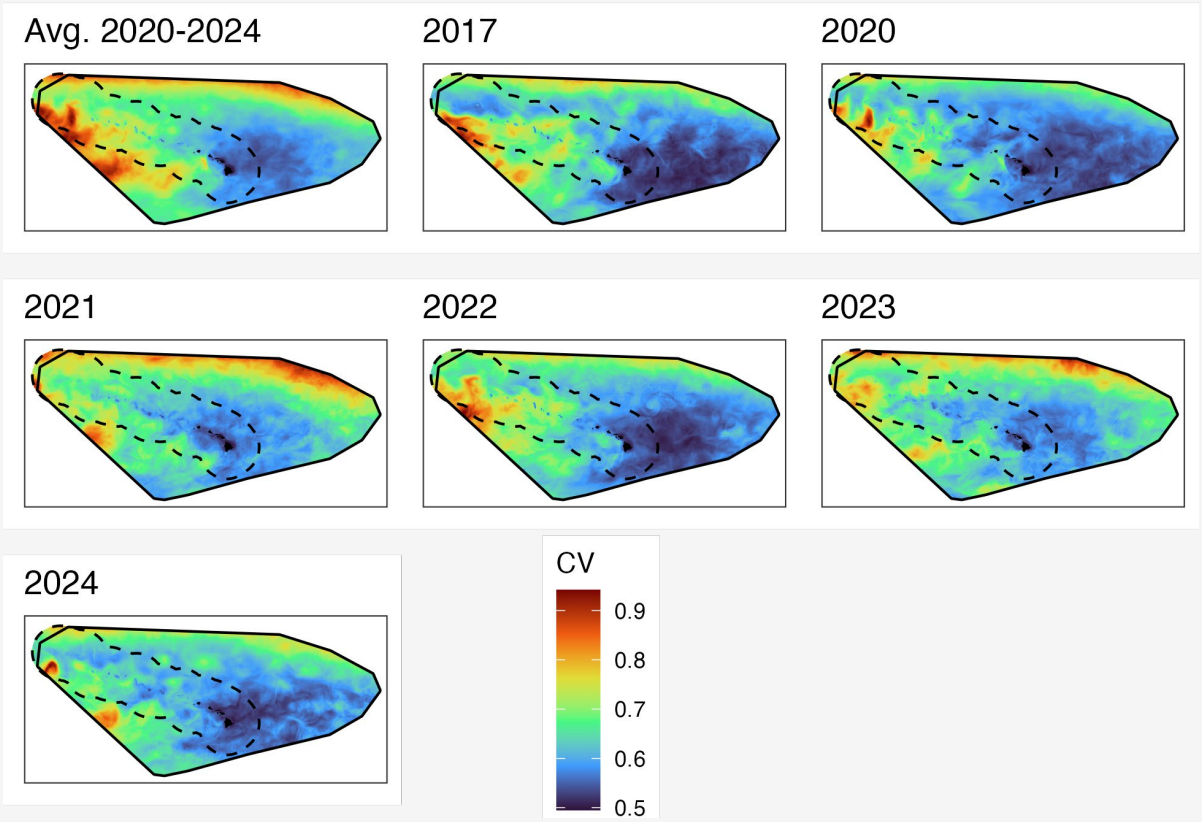

Figure 11. Spatially-explicit estimates of the abundance prediction coefficient of variation (CV) for pelagic false killer whale abundance in the U.S. Exclusive Economic Zone around the Hawaiian Islands (dashed line) and Hawai‘i pelagic false killer whale assessment area (solid line). Pixel color represents the CV in each pixel. Survey effort tracks are overlayed in this figure on the linked vignette.

Appendix A: Full Model Results

Encounter Rate Model

Top AIC model

```
Family: Tweedie(p=1.01)
Link function: log

Formula:
nSI_033 ~ te(sst, Latitude, bs = "ts") + s(ssh, bs = "ts") +
    s(ssh_sd, bs = "ts") + s(salinity_sd, bs = "ts")

Parametric coefficients:
            Estimate Std. Error t value Pr(>|t|)
(Intercept)  -8.9841     0.1863  -48.23   <2e-16 ***
---
Signif. codes:  0 ‘***’ 0.001 ‘**’ 0.01 ‘*’ 0.05 ‘.’ 0.1 ‘ ’ 1

Approximate significance of smooth terms:
                    edf Ref.df     F  p-value
te(sst,Latitude) 3.7468     24 0.877 2.15e-05 ***
s(ssh)           0.3150      9 0.043    0.242
s(ssh_sd)        0.5138      9 0.121    0.143
s(salinity_sd)   0.4988      9 0.133    0.118
---
Signif. codes:  0 ‘***’ 0.001 ‘**’ 0.01 ‘*’ 0.05 ‘.’ 0.1 ‘ ’ 1
```

```
R-sq.(adj) =  -8.86e-06   Deviance explained = 5.93%
-REML = 199.76  Scale est. = 1.0711    n = 14399
```

Prediction Model

```
Family: Tweedie(p=1.01)
Link function: log

Formula:
nSI_033 ~ te(sst, Latitude, bs = spline2use, k = 5)

Parametric coefficients:
            Estimate Std. Error t value Pr(>|t|)
(Intercept)  -8.9613     0.1844  -48.59   <2e-16 ***
---
Signif. codes:  0 ‘***’ 0.001 ‘**’ 0.01 ‘*’ 0.05 ‘.’ 0.1 ‘ ’ 1

Approximate significance of smooth terms:
                   edf Ref.df     F  p-value
te(sst,Latitude) 3.758     24 0.844 6.28e-05 ***
---
Signif. codes:  0 ‘***’ 0.001 ‘**’ 0.01 ‘*’ 0.05 ‘.’ 0.1 ‘ ’ 1

R-sq.(adj) =  -0.000392   Deviance explained = 4.92%
-REML = 200.23  Scale est. = 1.0716    n = 14399
```

Standard model checks:

```
Method: REML   Optimizer: outer newton
```

```
full convergence after 18 iterations.
Gradient range [-0.0008121005,5.945633e-05]
(score 200.2306 & scale 1.071581).
Hessian positive definite, eigenvalue range [5.945613e-05,3544.944].
Model rank =  25 / 25

Basis dimension (k) checking results. Low p-value (k-index<1) may
indicate that k is too low, especially if edf is close to k'.

                     k'   edf k-index p-value
te(sst,Latitude) 24.00  3.76    0.82   0.015 *
---
Signif. codes:  0 ‘***’ 0.001 ‘**’ 0.01 ‘*’ 0.05 ‘.’ 0.1 ‘ ’ 1
```

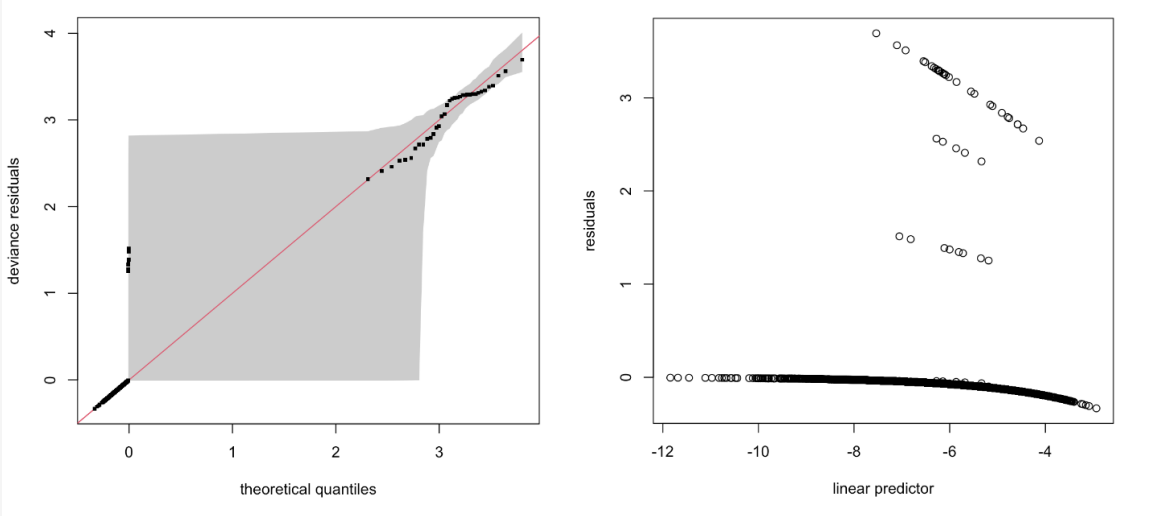

Figure A1. Figures from standard model checks for the encounter rate model, including randomized quantile residuals (left panel) and deviance residuals (right panel).

Group Size Model

Top AIC and Prediction Model

```
Family: gaussian
Link function: identity

Formula:
log(ANI_033) ~ s(ssh, bs = "ts") + s(mld, bs = "ts")

Parametric coefficients:
            Estimate Std. Error t value Pr(>|t|)
(Intercept)  1.63678    0.08493   19.27   <2e-16 ***
---
Signif. codes:  0 ‘***’ 0.001 ‘**’ 0.01 ‘*’ 0.05 ‘.’ 0.1 ‘ ’ 1

Approximate significance of smooth terms:
          edf Ref.df     F p-value
s(ssh) 0.9368      9 0.905 0.00435 **
s(mld) 0.9243      9 1.000 0.00291 **
---
Signif. codes:  0 ‘***’ 0.001 ‘**’ 0.01 ‘*’ 0.05 ‘.’ 0.1 ‘ ’ 1

R-sq.(adj) =  0.255   Deviance explained = 28.7%
-REML =  43.82  Scale est. = 0.2551    n = 44
```

Standard model checks:

```
Method: REML   Optimizer: outer newton
```

```
full convergence after 7 iterations.
Gradient range [-2.319745e-07,1.096197e-07]
(score 43.81978 & scale 0.2551005).
Hessian positive definite, eigenvalue range [0.3701801,21.52049].
Model rank =  19 / 19

Basis dimension (k) checking results. Low p-value (k-index<1) may
indicate that k is too low, especially if edf is close to k'.

          k'   edf k-index p-value
s(ssh) 9.000 0.937    1.09    0.62
s(mld) 9.000 0.924    1.25    0.91
```

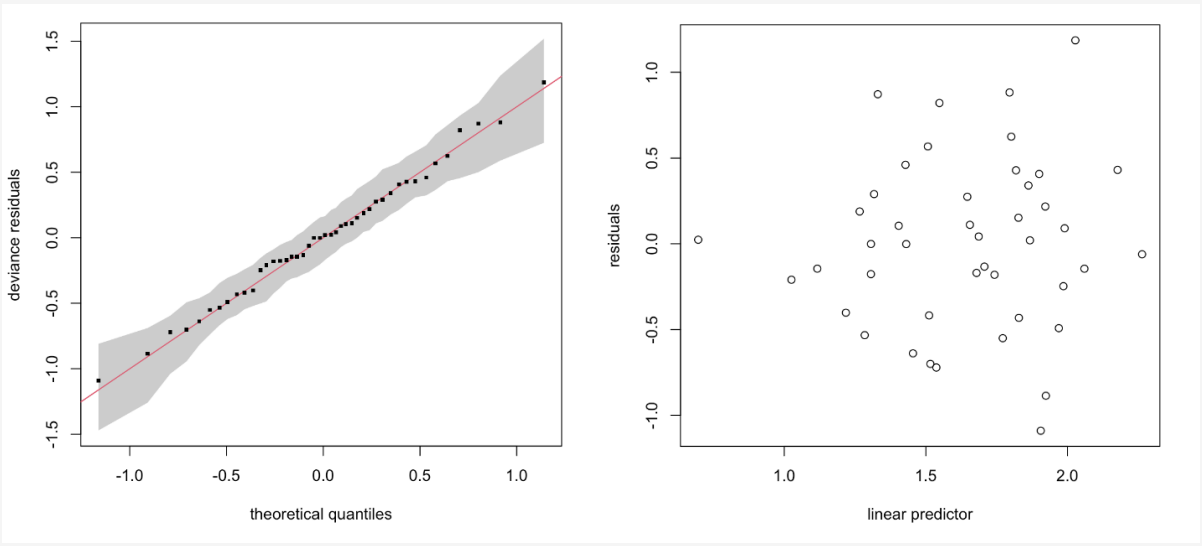

Figure A2. Figures from standard model checks for the group size model, including randomized quantile residuals (left panel) and deviance residuals (right panel).

Appendix B: Abundance Sensitivity to Model Selection

Table B1. AIC and percent deviance (%Dev) explained by selected pelagic false killer whale encounter rate models. Rank refers to their rank relative to 767 possible models using environmental covariates. Selection was chosen to show a range of model forms with similar AIC and %Dev among the 767 possible forms.

Rank	Formula	AIC	%Dev
1	~ SST*LAT + SSH + SD(SSH) + SAL	397.5	5.9
33	~ SST*LAT + SD(SST) + SAL	398.0	5.6
112	~ SST*LAT	399.0	4.9
321	~ MLD*LAT + SST + MLD + SD(SAL)	401.6	3.9

Table B2. AIC and percent deviance (%Dev) explained by selected pelagic false killer whale group size models. Rank refers to their rank relative to 16 possible models using environmental covariates. After non-significant terms are removed, only the top GS model remains, as other covariate terms (SST, SAL) were nonsignificant.

Rank	Formula	AIC	%Dev
1	~ SSH + MLD	85.7	28.7
2	~ SST+ SSH + MLD + SAL	85.7	28.7
3	~ SST + SSH + MLD	85.7	28.7
4	~ SSH + MLD + SAL	85.7	28.7
5	~ MLD + SAL	92.8	12.4

Table B3. Predicted pelagic false killer whale abundance in 2024 using encounter rate models from Table B1 and the top group size model from Table B2. Variance propagation was not performed for this sensitivity analysis, so the 95% confidence intervals (CIs) reported below are not comparable to those reported in Table 4.

ER Model	Central Pacific abundance [95% CI]	Assessment area abundance [95% CI]	Hawaiian EEZ abundance [95% CI]
1	36,117 [19,737–52,497]	4,869 [3,235–6,503]	1,881 [1,203–2,559]
33	35,739 [19,009–52,429]	4,762 [3,030–6,494]	1,813 [1,103–2523]
112	35,634 [18,962–52,576]	4,843 [2,951–6,735]	1,848 [1,106–2,950]
312	28,740 [18,864–38,616]	5,220 [2,534–7,906]	2,202 [1,008–3,396]

Appendix C: Models with Biological Covariates

As we are not able to include the full complement of biological variables (listed in Table C1) in the GAM models, we performed a principal components analysis to extract axes of variation in the biological data to include as covariates. We included the first and second components, together describing over 50% of the variation in provided biological data, as covariates in the GAMs describing encounter rate and group size. We found that while these variables increased percent deviance explained in encounter rate and group size (6.06% and 30.1% versus 4.92% and 28.7%, respectively), the associated parameters were not statistically significant. Thus, the biological variables did not meet our criteria to be included in the final models.

Data Description

The data set of biological variables is a reanalysis product from the Copernicus Marine Service that uses the low and mid-trophic component of SEAPODYM dynamical population model to provide a comprehensive global hindcast of biological variables at a 9-km spatial resolution, delivering daily estimates of net primary productivity, euphotic zone depth, and the biomass dynamics of zooplankton and micronekton. The model simulates these populations by categorizing taxa into functional groups based on their distribution within three vertical layers: the epipelagic, upper mesopelagic, and lower mesopelagic. While zooplankton is represented as a single carbon-based group (g/m2) restricted to the epipelagic layer, the micronekton component (spanning fish, crustaceans, squid, and gelatinous species in the 2–20 cm size range) is detailed through six distinct wet-weight groups (g/m2).

The micronekton variables are differentiated by their residency and vertical migration patterns throughout the water column. Three groups are defined as permanent residents of their respective layers (epipelagic, upper mesopelagic, and lower mesopelagic). The remaining three groups represent migrant populations: those moving between the upper mesopelagic and epipelagic, those moving between the lower and upper mesopelagic, and a "highly migrant" group that travels directly from the lower mesopelagic to the epipelagic layer during night-day alternations. Together with net primary productivity (mg/m2/day) and euphotic depth (m), these variables offer high-resolution modeled variables representing the energy transfer and spatio-temporal biomass density across the world’s oceans.

Table C1. Summary of biological variables considered during the pelagic false killer whale density surface modeling effort.

Variable	Long Name	Units	Description and Functional Grouping
zooc	Mass content of zooplankton	[g/m2] (C)	Total zooplankton biomass expressed in carbon; modeled as a single group in the epipelagic layer.
mnkc_epi	Epipelagic micronekton	[g/m2] (WW)	Permanent residents of the epipelagic layer (surface).
mnkc_umeso	Upper mesopelagic micronekton	[g/m2] (WW)	Permanent residents of the upper mesopelagic layer.
mnkc_lmeso	Lower mesopelagic micronekton	[g/m2] (WW)	Permanent residents of the lower mesopelagic layer.
mnkc_mumeso	Migrant upper mesopelagic micronekton	[g/m2] (WW)	Diel Migrants: Reside in the upper mesopelagic by day; migrate to the epipelagic by night.
mnkc_mlmeso	Migrant lower mesopelagic micronekton	[g/m2] (WW)	Diel Migrants: Reside in the lower mesopelagic by day; migrate to the upper mesopelagic by night.
mnkc_hmlmeso	Highly migrant lower mesopelagic micronekton	[g/m2] (WW)	Diel Migrants: Reside in the lower mesopelagic by day; migrate to the epipelagic by night.
npp	Net primary productivity	mg/m2/d	Rate of carbon fixation by phytoplankton.
zeu	Euphotic zone depth	m	Depth at which light intensity falls to 1% of the surface value.

Code

Principal Components Analysis

```
pca<-prcomp(~zooc+
              mnkc_epi+
              mnkc_umeso+
              mnkc_mumeso+
              mnkc_lmeso+
              mnkc_mlmeso+
              mnkc_hmlmeso+
              npp+
              zeu,
            data = fkw_dsm_data_bio, scale = TRUE)


(loadings <- pca$rotation)


axes <- predict(pca, newdata = fkw_dsm_data_bio)
fkw_dsm_data_bio_pc <- cbind(fkw_dsm_data, axes)
```

Encounter rate model

```
er_fit <- gam(formula = nSI_033 ~ te(sst, Latitude, bs = spline2use)+
                s(PC1) + s(PC2),
              offset = log(effort),
              family = tw(),
              method="REML",
              data = fkw_dsm_data, weights = ProbPel)
summary(er_fit)
```

```
Family: Tweedie(p=1.01)

Link function: log


Formula:

nSI_033 ~ te(sst, Latitude, bs = spline2use) + s(PC1) + s(PC2)


Parametric coefficients:

            Estimate Std. Error t value Pr(>|t|)

(Intercept)  -9.0478     0.2158  -41.92   <2e-16 ***

---

Signif. codes:  0 ‘***’ 0.001 ‘**’ 0.01 ‘*’ 0.05 ‘.’ 0.1 ‘ ’ 1


Approximate significance of smooth terms:

                   edf Ref.df     F  p-value

te(sst,Latitude) 2.640  24.00 0.610 0.000221 ***

s(PC1)           1.958   2.52 1.237 0.279298

s(PC2)           1.000   1.00 0.738 0.390358

---

Signif. codes:  0 ‘***’ 0.001 ‘**’ 0.01 ‘*’ 0.05 ‘.’ 0.1 ‘ ’ 1


R-sq.(adj) =  -0.000155   Deviance explained = 6.06%

-REML = 191.37  Scale est. = 1.0711    n = 13714
```

Group size model

```
gs_fit <- gam(formula = log(ANI_033) ~ s(ssh, bs = spline2use) +
s(mld, bs = spline2use)+

+                s(PC1) + s(PC2),

+              method="REML",
```

```
+              data = fkw_gs, weights = ProbPel)
summary(gs_fit)

summary(gs_fit)

Family: gaussian
Link function: identity

Formula:
log(ANI_033) ~ s(ssh, bs = spline2use) + s(mld, bs = spline2use) +
    s(PC1) + s(PC2)

Parametric coefficients:
            Estimate Std. Error t value Pr(>|t|)
(Intercept)   1.6274     0.0895   18.18   <2e-16 ***
---
Signif. codes:  0 ‘***’ 0.001 ‘**’ 0.01 ‘*’ 0.05 ‘.’ 0.1 ‘ ’ 1

Approximate significance of smooth terms:
          edf Ref.df     F p-value
s(ssh) 0.9252      9 0.837 0.00590 **
s(mld) 0.8955      9 0.771 0.00757 **
s(PC1) 1.0001      1 0.030 0.86296
s(PC2) 1.0000      1 0.030 0.86293
---
Signif. codes:  0 ‘***’ 0.001 ‘**’ 0.01 ‘*’ 0.05 ‘.’ 0.1 ‘ ’ 1
```

```
R-sq.(adj) =  0.229   Deviance explained = 30.1%
-REML = 44.565  Scale est. = 0.27293   n = 42
```